Cancer Biol Med 2025. doi: 10.20892/j.issn.2095-3941.2025.0014

ORIGINAL ARTICLE

Cancer cell-derived migrasomes harboring ATF6 promote breast cancer brain metastasis *via* endoplasmic reticulum stress-mediated disruption of the blood-brain barrier

Song Wang[1,2]*, Guohao Gu[1,2]*, Xinmiao Xian[1,2], Jun Li[1,2], Di Zhang[1,2], Jianran Guo[1,2], Anqi Zhang[3], Shen Chen[4], Dong Yan[1,2], Bingwu Yang[1,2], Meng An[5], Wei Zhang[4], Bo Fu[1,2]

[1]Department of Precision Biomedical Key Laboratory, Liaocheng People's Hospital, Liaocheng Hospital Affiliated to Shandong First Medical University, Liaocheng 252000, China; [2]Shandong Provincial Key Medical and Health Laboratory of Precision Medicine for Aging Intervention and Active Health, Liaocheng 252000, China; [3]Department of Central Laboratory, Liaocheng People's Hospital, Liaocheng Hospital Affiliated to Shandong First Medical University, Liaocheng 252000, China; [4]Department of Breast and Thyroid Surgery, Liaocheng People's Hospital, Liaocheng Hospital Affiliated to Shandong First Medical University, Liaocheng 252000, China; [5]Department of Clinical Laboratory, Liaocheng People's Hospital, Liaocheng Hospital Affiliated to Shandong First Medical University, Liaocheng 252000, China

ABSTRACT

Objective: Migrasomes, an emerging class of migration-facilitating membranous extracellular vesicles, remain largely uncharted in the intricate landscape of tumor metastasis. This study aimed to illuminate the roles and mechanisms underlying cancer cell-derived migrasomes in breast cancer brain metastasis (BCBM).

Methods: Migrasomes were isolated and purified from BCBM cells (231-BR) and non-specific organotropic parental counterparts (MDA-MB-231), specifically designated as Mig-BCBM and Mig-BC, respectively. The role of Mig-BCBM in BCBM was investigated using an *in vitro* endothelial cell layer permeability model and a BCBM mouse model. The regulatory mechanism underlying Mig-BCBM was assessed using RT-qPCR, western blotting, immunofluorescence, *ex vivo* fluorescence imaging, and a series of rescue experiments.

Results: Mig-BCBM potently augmented the permeability of vascular endothelial layers, which facilitated the efficient migration of 231-BR cells across endothelial barriers *in vitro*. The administration of Mig-BCBM significantly disrupted the blood-brain barrier (BBB) and accelerated BCBM progression *in vivo*, as evidenced in mouse models, compared to the Mig-BC and control groups. Mechanistically, Mig-BCBM harbored ATF6, a critical transducer of endoplasmic reticulum (ER) stress. Upon internalization into hCMEC/D_3 cells, ATF6 elicited robust ER stress responses, culminating in downregulation of ZO-1 and VE-cadherin. Digital PCR analysis disclosed significant upregulation of ATF6 in serum migrasomes derived from BCBM patients compared to migrasomes from breast cancer patients and healthy individuals.

Conclusions: This study uncovered a pivotal role of cancer cell-derived in BCBM by harnessing ATF6-mediated ER stress to disrupt the BBB and promote metastasis, suggesting novel diagnostic and therapeutic strategies targeting migrasomes and migrasome cargo.

KEYWORDS Breast cancer brain metastasis; migrasome; blood-brain barrier; ATF6; endoplasmic reticulum stress

Introduction

Breast cancer (BC), an ominous malignancy, ranks second in frequency as a precursor to brain metastasis, which poses a formidable challenge to healthcare[1]. Nearly 25% of advanced BC patients have a devastating complication (brain metastasis)[2]. Breast cancer brain metastasis (BCBM) is associated with a poor prognosis and impairs cognitive and sensory functions, which leading to a severely limited quality of life[3]. Currently, a multidisciplinary arsenal of therapeutic strategies, including surgical excision, radiation therapy, chemotherapy, and

*These authors contributed equally to this work.
Correspondence to: Meng An, Wei Zhang and Bo Fu
E-mail: 2008anmeng2008@163.com, zhangw1972@126.com and fubo.22@163.com
ORCID ID: https://orcid.org/0000-0003-2908-3199, https://orcid.org/0009-0000-4419-7691 and https://orcid.org/0000-0002-6584-391X
Received January 8, 2025; accepted April 21, 2025; published online June 9, 2025.
Available at www.cancerbiomed.org
©2025 The Authors. Creative Commons Attribution-NonCommercial 4.0 International License

combinations of the therapeutic strategies, are used to combat BCBM[4]. Nevertheless, the life expectancy of patients with BCBM is unsatisfactory due to the blood-brain barrier (BBB), which restricts penetrability of bioactive compounds[2,5]. Therefore, there is an urgent need to elucidate the molecular mechanisms underlying BCBM, with the aim of discovering novel therapeutic targets, enhancing treatment efficacy, and ultimately improving patient prognosis.

Organ-specific metastasis is contingent upon the establishment of a pre-metastatic niche (PMN) by primary tumors, crafting a hospitable microenvironment in secondary organs conducive to metastatic tumor cell colonization and settlement[6]. Prior to dissemination, primary tumor-derived extracellular vesicles have a crucial role in shaping the PMN, profoundly impacting cancer progression and ultimate outcomes[7]. Migrasomes, a recently discovered cellular substructure, originate from retraction fibers (RFs) of migratory cells, marking a novel frontier in cellular biology[8-10]. Recent investigations have confirmed the ubiquitous presence of migrasomes in regions of cellular migration and motility across diverse organisms. As cells embark on their migratory journey, migrasomes remain stationary, either rupturing or being internalized by adjacent cells, thereby disseminating vital components, such as mRNA and protein from the donor cells[11,12]. Migrasomes also remain on the migration path of migrating cells, acting as positioning signals after the cells have left[13]. This unique ability enables migrasomes to integrate biological and spatial cues, propagate composite signals, and orchestrate intercellular communication. Recent studies have shown that migrasomes are involved in the regulation of intracellular mitochondrial homeostasis through migratory exocytosis[14]. Zhang et al. demonstrated that CD151-enriched migrasomes facilitate hepatocellular carcinoma invasion by conditioning cancer cells and promoting angiogenesis[15]. Pancreatic cancer cell-derived migrasomes (PCDMs) promote cancer progression by fostering an immunosuppressive microenvironment[16]. Wang et al.[17] discovered the presence of PD-L1 in a significant number of migrasomes that facilitate cancer cell migration. Because the functional exploration of migrasomes is still a work in progress, the intricate mechanisms by which migrasomes influence the formation of PMN, especially in BCBM, have not been established.

Brain metastasis formation is uniquely characterized by exclusive entry through the BBB, a unique brain feature that serves as the sole pathway for circulating tumor cells and is thus the primary focus of the brain PMN[18,19]. The BBB, which is predominantly composed of brain microvascular endothelial cells, a basement membrane, pericytes, and astrocyte foot processes, functions as a vital guardian of the brain' microenvironment[20,21]. The unique intercellular architecture and anatomic configuration of the BBB uphold the delicate balance of brain' homeostasis by rigorously regulating the influx of exogenous macromolecules and cells into the brain parenchyma[20]. Accumulating evidence has demonstrated that tight junctions and adherens junctions of cerebral vascular endothelial cells have a major role in BBB permeability[22,23]. The tight junction-associated protein zone occluding-1 (ZO-1) and adherens junctions-associated membrane protein (VE-cadherin) are expressed in cerebral vascular endothelial cells and are indispensable for maintaining BBB integrity[24,25].

The endoplasmic reticulum (ER) has a crucial role in protein synthesis, maturation, and trafficking[26,27]. Disruption of ER homeostasis results in the accumulation of unfolded or misfolded proteins, which triggers ER stress[28]. The unfolded protein response (UPR) ensures quality control by upregulating ER chaperones in response to ER stress, suppressing other protein synthesis and eliminating misfolded proteins[26,29]. UPR activation is orchestrated by inositol-requiring enzyme 1 (IRE-1), protein kinase R-like endoplasmic reticulum kinase (PERK), and activating transcription factor 6 (ATF6)[30,31]. The 78 kDa glucose-regulated protein (GRP78), an ER chaperone, binds to ATF6, PERK, and IRE-1 to inhibit activity in the absence of stress. GRP78 dissociates from these sensors under stress, binds to unfolded proteins, and activates the UPR. Upon release from GRP78, ATF6 translocates to the Golgi, where ATF6 is cleaved and moves to the nucleus to activate genes, including GRP78, GRP79, and X-box binding protein 1 (XBP1)[32,33]. Aberrant activation of UPR/ER stress has emerged as a pivotal regulator of tumor growth, metastasis, and relapse[29,31,34].

In the present study, we formulated a hypothesis positing that migrasomes derived from BCBM cells may contribute to brain metastases progression by disrupting the integrity of vascular endothelial barriers and augmenting BBB permeability *via* ER stress. Migrasomes emanating from brain metastatic breast cancer cells (231-BR) and the non-specific organotropic parental counterparts (MDA-MB-231) were isolated and characterized, and specifically designated as Mig-BCBM and Mig-BC, respectively. Mig-BCBM significantly potentiated BBB permeability, thereby facilitating the development of BCBM. Our study revealed that Mig-BCBM downregulates ZO-1 and VE-cadherin levels in cerebral vascular endothelial

cells (hCMEC/D_3) by inducing ER stress *via* the delivery of ATF6. This study uncovered novel molecular underpinnings of BCBM and shed light on potential prognostic biomarkers as well as therapeutic targets.

Material and methods

Patients and samples

A total of 109 retrospective plasma samples were included in this study, including 32 samples from BCBM patients, 36 samples from BC patients, and 41 samples from individuals with no evidence of disease and serving as healthy controls. The sample size was determined using G*Power software (effect size = 0.4, α = 0.05, and power = 0.8) with a minimum requirement of 22 samples per group. These plasma specimens were collected before any interventional procedures were performed at Liaocheng People's Hospital, Liaocheng Hospital Affiliated to Shandong First Medical University (Liaocheng, Shandong, China) from June 2019 to March 2023. As part of the screening process, the inclusion and exclusion criteria were as follows: (1) the BCBM group included patients with confirmed BCBM based on imaging or pathology findings and excluded patients with other malignancies (excluding breast cancer) or brain diseases (e.g., stroke and encephalitis); (2) the BC group included patients with pathologically confirmed BC and excluded patients with metastases or other malignancies (excluding breast cancer); and (3) the healthy control group included healthy individuals without any neoplasms, excluding individuals with chronic diseases (e.g., diabetes and hypertension) or recent infections and inflammatory conditions. Ethical approval was obtained from the Ethics Committee of Liaocheng Hospital Affiliated to Shandong First Medical University (Approval no. R2022035). All the participants provided written informed consent.

Cell culture

The cell source and culture conditions of the human brain-targeting breast carcinoma cell line, 231-BR, and its parental cell line, MDA-MB-231, were as described previously[35-37]. The human brain microvascular endothelial cell line, hCMEC/D_3 (Mingzhoubio, Zhejiang, China), was cultured in basic medium supplemented with 5% fetal bovine serum (FBS), 1% endothelial cell culture additive for endothelial cell culture, and 1% penicillin-streptomycin in 5% CO_2 at 37°C.

Animal model

All animal experimental protocols were approved by the Laboratory Animal Welfare and Ethics Committee of Liaocheng People's Hospital (Approval no. D2022057) and performed according to the Guide for the Care and Use of Laboratory Animals. Female BALB/c nude mice (8 weeks old weighing 18–20 g; Vital River Laboratory Animal Technology, Beijing, China) were bred and housed at a controlled temperature (22 ± 1°C) and exposed to a constant 12 h light-dark cycle in the animal facility.

Mig-BCBM and Mig-BC were injected into mice *via* tail veins at a concentration of 200 μg/mL twice weekly to evaluate the effects of migrasomes on BCBM. Four weeks later, the BCBM mouse models were established by injecting 231-BR or $^{GFP+}$231-BR cells into the left ventricles, as described previously[35].

BBB integrity evaluation

Two percent Evans blue [EB] (2 mL/kg) was injected through tail veins 2 h prior to sacrificing the mice. Specifically, the mice were anesthetized with an intraperitoneal injection of 1% pentobarbital sodium (50 mg/kg) before removing excess EB by trascardial perfusion with 200–300 mL of heparin saline (0.9% sodium chloride and 20 U/mL heparin sodium). The mice were decapitated and the brains were collected for sagittal cutting after removing the hippocampus. One hemisphere was frozen sectioned for a BBB integrity examination. EB penetration, which indicated BBB permeability, was photographed using a fluorescence microscope (Olympus Corp., Tokyo, Japan). The other half-hemisphere was used to evaluate the EB amount. The half-hemisphere was weighed, grinded, placed in dimethylformamide (1 ml dimethylformamide per 100 mg brain tissue), incubated at 60°C for 24 h, centrifuged at 94 g for 5 min, and the absorbance at 620 nm was measured with a spectrophotometer. EB standard curve was drawn to calculate EB content.

Isolation of migrasomes

Previously established protocols[38] were refined and adapted to isolate migrasomes from cultured cells or human serum samples. Cells were cultured in fibronectin-coated 150 mm dishes and collected into 50 mL tubes for isolation from cultured cells. In the case of human serum samples, a 5-mL serum sample per individual was centrifugated at 845 g for 10 min.

Large debris in the pellets were subsequently removed by centrifugation at 1,000 *g* for 10 min followed by 4,000 *g* for 20 min. After centrifuging at 20,000 *g* for 30 min, pellets were collected as crude migrasomes. To obtain precise migrasome fractionation, density gradient centrifugation was performed utilizing an OptiPrep kit (LYSISO1; Sigma-Aldrich, city, state, country). The crude migrasome pellets were resuspended with 650 μL of Optiprep dilution buffer, then mixed with 400 μL of 1 × extraction buffer, 30 μL of 2.3 M sucrose, and 505 μL of 60% OptiPrep, compounding 1,585 μL of crude migrasome suspension with 19% Optiprep. Then, a step gradient was built starting with 27% (800 μL), followed by 22.5% (1,000 μL), crude migrasome resuspension (19%, 1,000 μL), 16% (1,000 μL), 12% (900 μL), and 8% (300 μL). The gradient was centrifuged at 150,000 *g* for 4 h in an MLS-50 rotor. Fractions were then separately collected from each gradient with volumes ranging from 500 to 700 μL. Each fraction was then diluted with an equal volume of PBS and centrifuged at 20,000 *g* for 30 min to isolate the migrasomes as pellets.

Transmission electron microscopy (TEM)

Migrasomes were gently resuspended in 20 μL PBS and fixed in an equal volume of 25% glutaraldehyde for 2 h for negative staining. The fixed migrasomes were absorbed onto a carbon-coated copper grid for 5 min and stained with a single drop of 2% phosphotungstic acid for 3 min. Finally, the grids were allowed to air-dry for 15 min and observed under a JEM-1200EX electron microscope (Jeol, Tokyo, Japan).

For resin-embedded ultrathin section staining, migrasomes isolated by density gradient centrifugation were fixed, pre-embedded in agarose, and post-fixed with 1% osmium tetroxide for 2 h. The samples were dehydrated using an ethanol-acetone series, infiltrated, and embedded in resin. Ultrathin sections (60–80 nm) were cut, collected on copper grids, and stained with 2% uranyl acetate (8 min) and 2.6% lead citrate [8 min (CO_2-free)]. After washing and drying, the sections were imaged by TEM for migrasome analysis.

Scanning Electron Microscopy (SEM)

Migrasomes was fixed with 25% glutaraldehyde for 2 h, followed by incubation for 12 h in a refrigerator at 4°C. The samples were then washed. After washing, the samples were dehydrated through a graded ethanol series (50%, 70%, 80%, 90%, 100%, 100%, and 100%). The dried samples were then mounted on copper plates and observed under a Hitachi SU8010 electron microscope (Hitachi, Tokyo, Japan).

Wheat-germ agglutinin (WGA) staining

Confocal Petri dishes (35 mm) were precoated with 2 μg/mL of fibronectin and incubated at 37°C for 6 h to facilitate cell attachment. The fibronectin solution was discarded after incubation. The digested cells were then seeded to attain a density of 30–40% and allowed to adhere for 20 h. The migrasomes were then stained with WGA[39]. Finally, images were captured using a confocal microscope (Leica Microsystems, Mannheim, Germany).

Western blotting

Proteins from cells, migrasomes, or mouse tissue were extracted in RIPA reagent. Protein concentrations were determined using a BCA protein assay kit (#P0010S; Beyotime, Beijing, China). Proteins were separated by 10–15% SDS-PAGE and transferred to polyvinylidene fluoride (PVDF) membranes. The membranes were blocked with 5% non-fat milk and incubated with primary antibodies against PIGK (#ab201693, 1:1,000; Abcam, Boston, MA, USA), CPQ (#000012845, 1:1,000; Sigma-Aldrich, St. Louis, MO, USA), ZO-1 (#13663, 1:1,000; Cell Signaling Technology, Danvers, MA, USA), VE-cadherin (#13116, 1:1,000; Cell Signaling Technology), or β-actin (#sc-47778, 1:1,000; Santa Cruz, CA, USA) overnight at 4°C. After washing with TBST, the membranes were incubated with HRP-conjugated secondary antibody [HRP-labeled goat anti-rabbit IgG (H+L), #A0208; Beyotime; HRP-labeled goat anti-mouse IgG (H+L), #A0216; Beyotime] at room temperature for 1 h. Protein-antibody complexes were visualized using an enhanced chemiluminescence reagent (#34580; Thermo Fisher Scientific, Waltham, MA, USA) and captured on a chemiluminescence imaging system (Tanon, Shanghai, China).

Real-time quantitative polymerase chain reaction (RT-qPCR)

Total RNA was extracted using Trizol reagent (Thermo Fisher Scientific) to quantify gene expression in brain tissues and cells. Specific primers of targeting sequences were designed and synthesized, as listed in **Table S1**. The first strand of complementary DNA (cDNA) was synthesized from the isolated RNA using a reverse transcription kit (Beyotime) following

the manufacturer's protocol. The cDNA was subjected to RT-qPCR using the TB Green Premix Ex Taq II kit (Takara, Dalian, China). The amplification mix contained 0.8 μL of forward primer (10 μM), 0.8 μL of reverse primer (10 μM), 2 μL of cDNA (50 ng/μL), 10 μL of 2 × master mix, 0.4 μL of ROX II, and 6 μL of ddH_2O. PCR was performed on the 7,500 Real-time PCR System (Applied Biosystems, Foster City, CA, USA).

Digital PCR (dPCR)

Migrasomes from serum samples of BCBM patients, BC patients, and healthy individuals were isolated. Total RNA was extracted from the migrasomes using TRIzol reagent (Thermo), followed by reverse transcription according to the instructions (Beyotime). cDNA was subjected to dPCR using a HQ dPCR EvaGreen Master Mix Kit (Sniper, Suzhou, China). dPCR amplification was performed on a dPCR system (Sniper), as described previously[40]. The amplification mix contained 8 μL of cDNA, 11 μL of 2 × dPCR EvaGreen Master Mix, 1.0 μL of upstream primer (10 μM), 1.0 μL of downstream primer (10 μM), and ddH_2O to adjust the total volume to 22 μL. The amplification conditions included incubation at 60°C for 5 min for droplet stabilization and activation of Taq enzyme at 95°C for 15 min. Each cycle consisted of denaturation at 95°C for 15 s and annealing/extension at 60°C for 30 s, which was repeated for a total of 40 cycles. Fluorescence signal acquisition was performed at 60°C for 60 s in a single cycle. The amplification curves were interpreted using SightPro software (Sniper).

Hematoxylin and eosin (H&E) staining

Mouse brain tissues were fixed with 4% paraformaldehyde for 24 h. Then, the brain tissues were embedded with paraffin and sectioned at a thickness of 5 μm. After dewaxing, the sections were stained with an H&E staining kit (Solarbio, Beijing, China). Brain metastatic nodules were counted under a microscope, as previously described[35].

4D label-free proteomics analysis

SDT buffer (composed of 4% SDS and 100 mM Tris-HCl at pH 7.6) facilitated sample lysis and protein extraction of migrasomes. LC-MS/MS analysis was performed on a Bruker timsTOF Pro mass spectrometer interfaced with a Nanoelute system. Peptides were loaded onto a 25 cm × 75 μm (i.d.), 1.9-μm resin C18 reversed-phase column (Thermo Fisher Scientific) in 95% buffer A (0.1% formic acid in water) and eluted with a linear gradient of buffer B (99.9% acetonitrile and 0.1% formic acid) at 300 nL/min. The mass spectrometer was operated in a positive ion mode with an electrospray voltage of 1.5 kV to analyze precursors and fragments within an m/z range of 100–1,700. The timsTOF Pro (company, city, state, country) was operated in the PASEF mode, with parameters set as follows: ion mobility coefficient (1/K0) range of 0.6–1.6 Vs cm^2; 1 MS scan followed by 10 MS/MS PASEF scans; and an active exclusion period of 24 s. Raw MS data for each sample were pooled and analyzed using MaxQuant 1.6.14 software for identification and quantitation.

Immunofluorescence (IF) staining

Cells were fixed with 4% paraformaldehyde for 30 min, then permeabilized with 0.5% Triton X-100 (company, city, state, country). After blocking with 5% BSA, the cells were incubated with primary antibodies for 1 h or overnight at 4°C. After washing, the cells were incubated with the secondary antibody for 60 min. The cells were then washed with PBS and stained with DAPI for 10 min. Images were captured under a BX53 microscope (Olympus, Tokyo, Japan).

Lentivirus infection

ATF6 gene knockdown in $hCMEC/D_3$ or 231-BR cells was achieved by infecting the cells with an shRNA containing lentivirus Lv-shATF6 (Genechem, Shanghai, China). Lv-shNC, which had no target gene, was used as the negative control. $hCMEC/D_3$ cells were infected with Lv-shATF6 or Lv-shNC at a multiplicity of infection (MOI) of 100 for 12 h according to the manufacturer's instructions. A selection process was performed with 2 μg/mL of puromycin (Beyotime) for 48 h to obtain the successfully infected cells. ATF6-knockdown migrasomes (Mig-shATF6) were subsequently isolated from the stable 231-BR cells with ATF6 knockdown for further analysis.

Endothelial cell layer permeability test

$hCMEC/D_3$ cells were seeded onto the polyethylene terephthalate membrane (0.4 μm pore size) in the upper chamber of a 24-well Transwell plate. The cells were allowed to grow and fuse, then treated with 8 μg/mL of Mig-BCBM for 48 h. After removing the culture medium from the upper chamber,

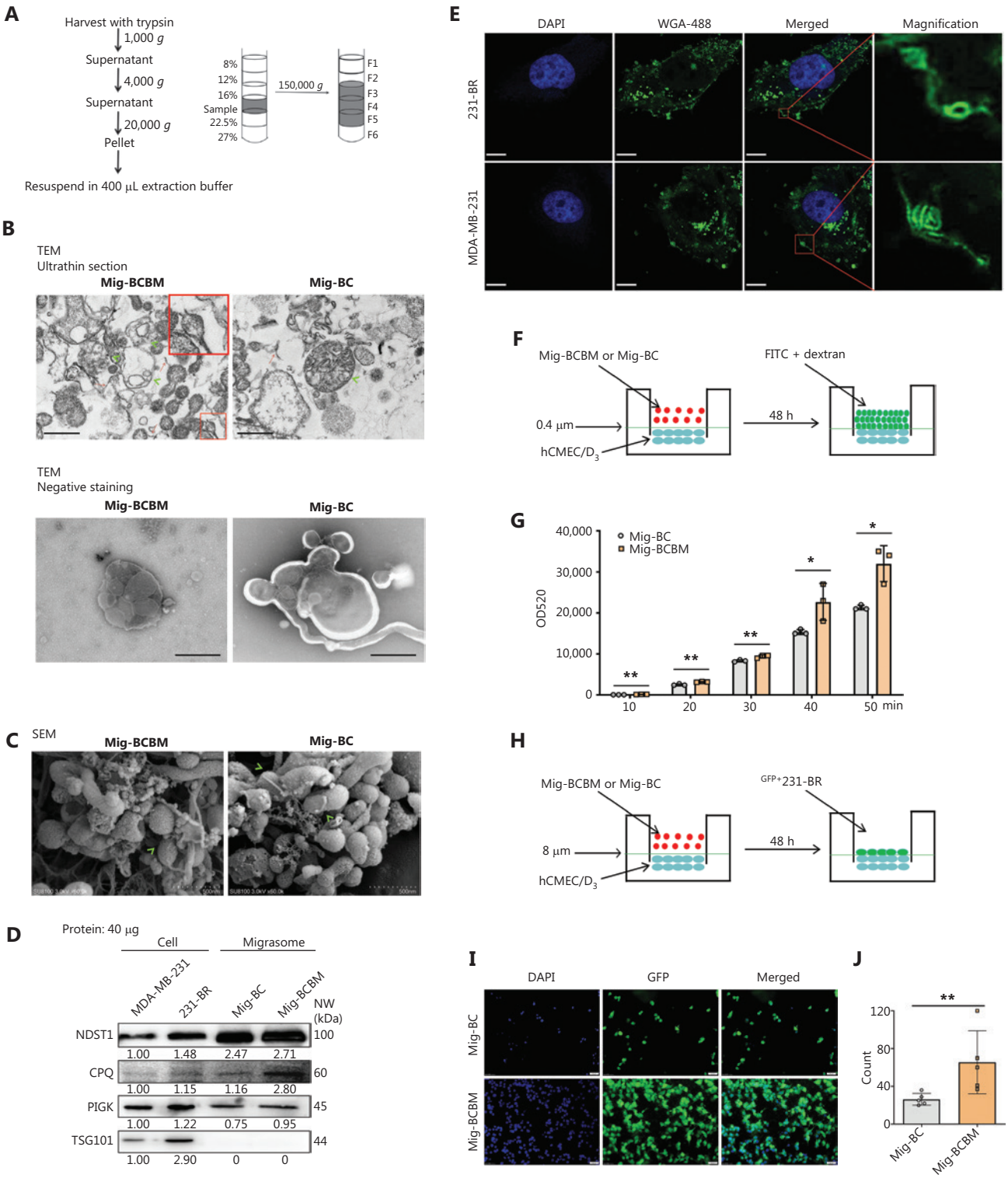


Figure 1 Mig-BCBM facilitates 231-BR cell migration through vascular endothelial layers *in vitro*. (A) Isolation and purification of migrasomes. 231-BR or MDA-MB-231 cell-derived migrasomes were isolated and purified using density gradient centrifugation. (B) TEM imaging of migrasomes. TEM revealed the ultrastructural features of isolated migrasomes. The green arrows indicate migrasomes. The red arrows indicate retraction fibers. In the left panel of the ultrathin section, the magnified view in the upper right corner corresponds to the area marked by the red box. Scale bars, 500 nm. (C) SEM visualization of migrasomes. The green arrows indicate migrasomes. Scale bar, 500 nm. (D) Western

blotting analysis of 231-BR or MDA-MB-231 cells and cell-derived migrasome Mig-BCBM and Mig-BC using antibodies against NDST1, CPQ, PIGK, and TSG101. 231-BR and MDA-MB-231 cells, along with Mig-BCBM and Mig-BC, were normalized with total protein. The grey values of the western blot bands were quantified using ImageJ software. (E) 231-BR or MDA-MB-231 cell-derived migrasomes were stained with WGA probes. The magnified images in the right panel correspond to the areas delineated by the red boxes. Scale bars, 5 μm. (F) Schematic of endothelial cell layer permeability assay. Polyethylene terephthalate membrane, 0.4 μm pore size. (G) Effect of Mig-BCBM on hCMEC/D_3 cell layer permeability. n = 3. (H) Schematic of $^{GFP+}$231-BR cell migration through vascular endothelial layers. Polyethylene terephthalate membrane, 8 μm pore size. (I) Effect of Mig-BCBM on the migration of 231-BR cells across vascular endothelial layers. Representative images of $^{GFP+}$231-BR cell migration through vascular endothelial layers. Scale bars, 50 μm. (J) Quantification of $^{GFP+}$231-BR cell migration through vascular endothelial layers. n = 5; *P < 0.05, **P < 0.01.

10 mg/mL of FITC-labeled dextran was added to the hCMEC/D_3 culture medium. The lower chamber was filled with 1 mL of hCMEC/D_3 culture medium. Fifty microliters of the culture medium in the lower chamber were withdrawn at each time point (10, 20, 30, 40, and 50 min). The optical density (OD) value was detected using a SpectraMax microplate multifunctional enzyme-linked immunosorbent assay reader (Molecular Devices, San Jose, CA, USA) with excitation and emission wavelengths set at 488 nm and 520 nm, respectively.

Tumor cell migration through the endothelial cell layer

hCMEC/D_3 cells were seeded at a density of 2×10^4 on polyethylene terephthalate films (8-μm pore size) within the upper chamber of a 24-well Transwell chamber. Following growth to confluence, the cells were treated with 8 μg/mL of Mig-BCBM for 48 h. The medium in the upper chamber was aspirated and GFP-transfected 231-BR cells were added (1×10^5/mL resuspended in 100 μL of serum-free high-glucose DMEM). The lower Transwell chamber was filled with 500 μL of high-glucose DMEM containing 10% FBS. The upper chamber was carefully removed and fixed in 4% paraformaldehyde following incubation for 12 h. After a gentle rinse with PBS, $^{GFP+}$231-BR cells and hCMEC/D_3 cells remaining in the upper chamber that had not migrated to the lower surface of the filter were gently removed using cotton swabs. The nuclei were stained with Hoechst 33,342 (Solarbio, Beijing, China) at a dilution of 1:5,000 for 10 min. Finally, the lower chamber of the filter was observed under an inverted fluorescence microscope and six random fields of view were photographed per well.

Ex vivo fluorescence imaging

Whole-brain *ex vivo* fluorescence images were captured using an IVIS Spectrum *in vivo* imaging system (PerkinElmer, Waltham, MA, USA)[41] with a red filter. The images were analyzed using Living Image software 4.4. The fluorescence signals were separated through the application of multispectral imaging technology.

Statistical analysis

All results were confirmed in at least three independent experiments. All quantitative data are presented as the mean ± standard deviation (SD). Statistical analysis was performed using GraphPad Prism 9 (San Diego, CA, USA) or SPSS26.0 software. For quantitative data, the distribution was assessed using the Shapiro-*W*ilk normality test. Comparisons between two groups were analyzed using the unpaired or paired *t*-test for normally distributed data, while comparisons among multiple groups were analyzed using one-way analysis of variance (ANOVA) followed by Tukey's *post-hoc* test for pairwise comparisons. The Mann-Whitney *U* test (for two groups) or the Kruskal-Wallis *H* test (for multiple groups) was applied for non-normally distributed data, followed by Dunn's test for pairwise comparisons. A $P < 0.05$ was considered statistically significant.

Results

Mig-BCBM promotes migration of 231-BR cells across vascular endothelial layers *in vitro*

The unique human 231-BR/MDA-MB-231 cell model with a syngeneic nature was utilized to investigate the functions of cancer-derived migrasomes. The MDA-MB-231 parental cells exhibited the ability to metastasize to diverse sites without organ specificity, whereas the 231-BR cell variant specifically targeted the brain. 231-BR cells metastasize exclusively to the brain with 100% specificity, making 231-BR cells a valuable preclinical research model for brain metastatic breast cancer[42].

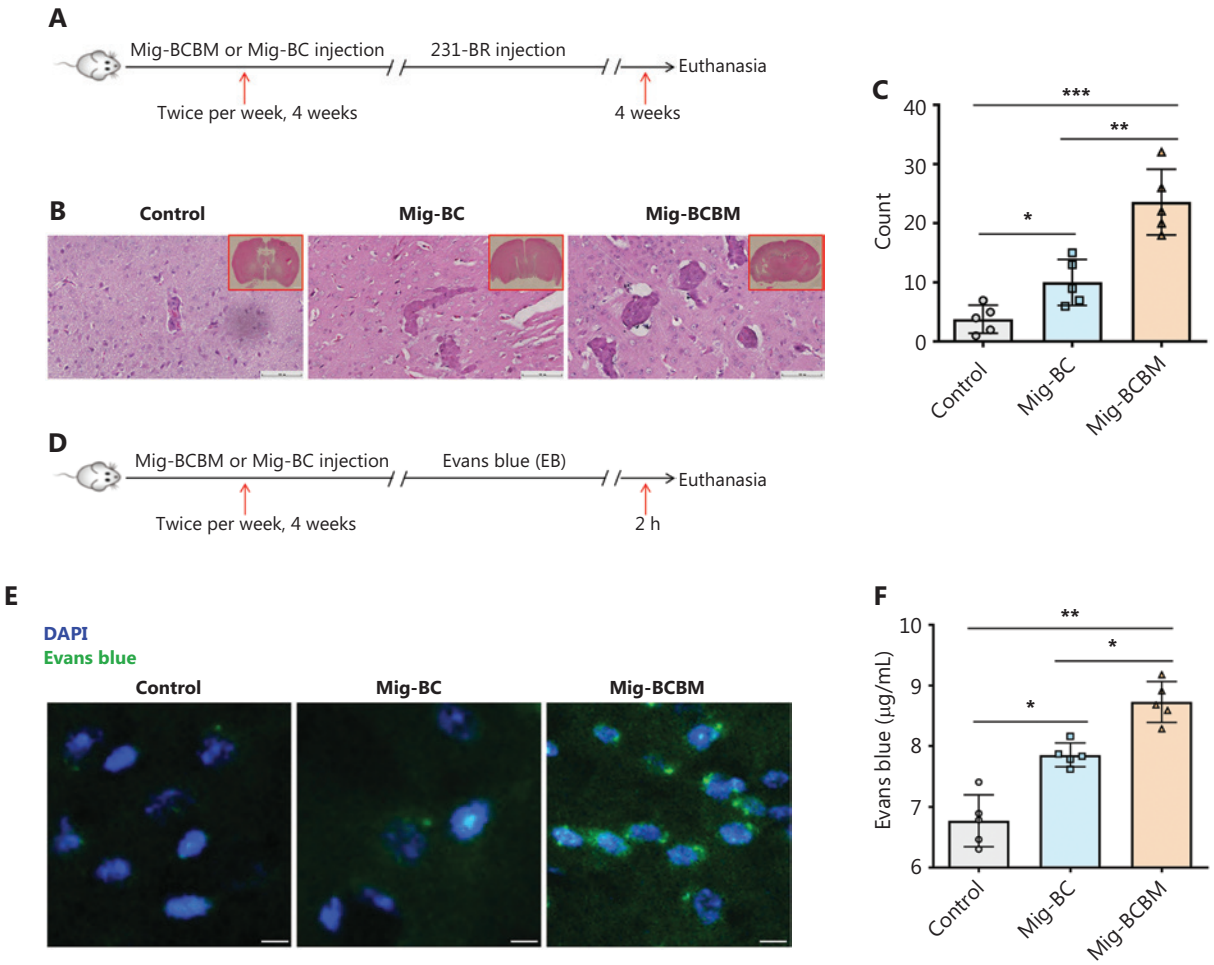


Figure 2 Mig-BCBM enhances BBB permeability and promotes BCBM *in vivo*. (A) Schematic illustration of a model designed to detect the effect of Mig-BCBM or Mig-BC on BCBM. (B and C) Effect of Mig-BCBM on BCBM *in vivo*. H&E staining of brain tissues (B) and quantification of brain metastases (C). Top right: H&E-stained whole brain section (scale bars, 1 mm). Brain metastasis nodule images (scale bars, 50 μm) show magnified view of black-framed area. $n = 5$. (D) Schematic illustration of a model designed to detect the effect of Mig-BCBM on disrupting BBB. (E and F) Effect of Mig-BCBM on BBB permeability. Evans blue (EB) fluorescence images (E) and concentration (F) in the brains. Scale bars, 10 μm. $n = 5$; $^*P < 0.05$, $^{**}P < 0.01$, $^{***}P < 0.001$.

Migrasomes derived from 231-BR and MDA-MB-231 cells were isolated and purified, and were designated as Mig-BCBM and Mig-BC, respectively (**Figure 1A**).

Migrasomes were identified using TEM, SEM, western blotting, and WGA staining (**Figure 1B-1E**). Under TEM, cancer-derived migrasomes were round or nearly round with membrane encapsulated and sizes ranged from 400 to 2,000 nm; some migrasomes had RFs (**Figure 1B**). SEM analysis further revealed the presence of RFs within some migrasomes (**Figure 1C**). Previous studies have demonstrated that NDST1, CPQ, and PIGK are enriched within migrasomes, whereas NDST1, CPQ, and PIGK are absent or barely detectable in exosomes, thus serving as migrasome-specific protein markers[38,43]. NDST1, CPQ, and PIGK proteins were effectively detected through western blotting in 231-BR and MDA-MB-231 cells and cell-derived migrasome Mig-BCBM and Mig-BC (**Figure 1D**). Conversely, the exosome marker, TSG101, was absent in Mig-BCBM and Mig-BC, confirming the successful isolation of migrasomes from the cultured cells. WGA can be utilized as an effective probe for migrasomes[39]. As shown in **Figure 1E**, migrasomes were conspicuously distributed around 231-BR and MDA-MB-231 cells. Taken together, these data indicated successful isolation of migrasomes from 231-BR and MDA-MB-231 cells.

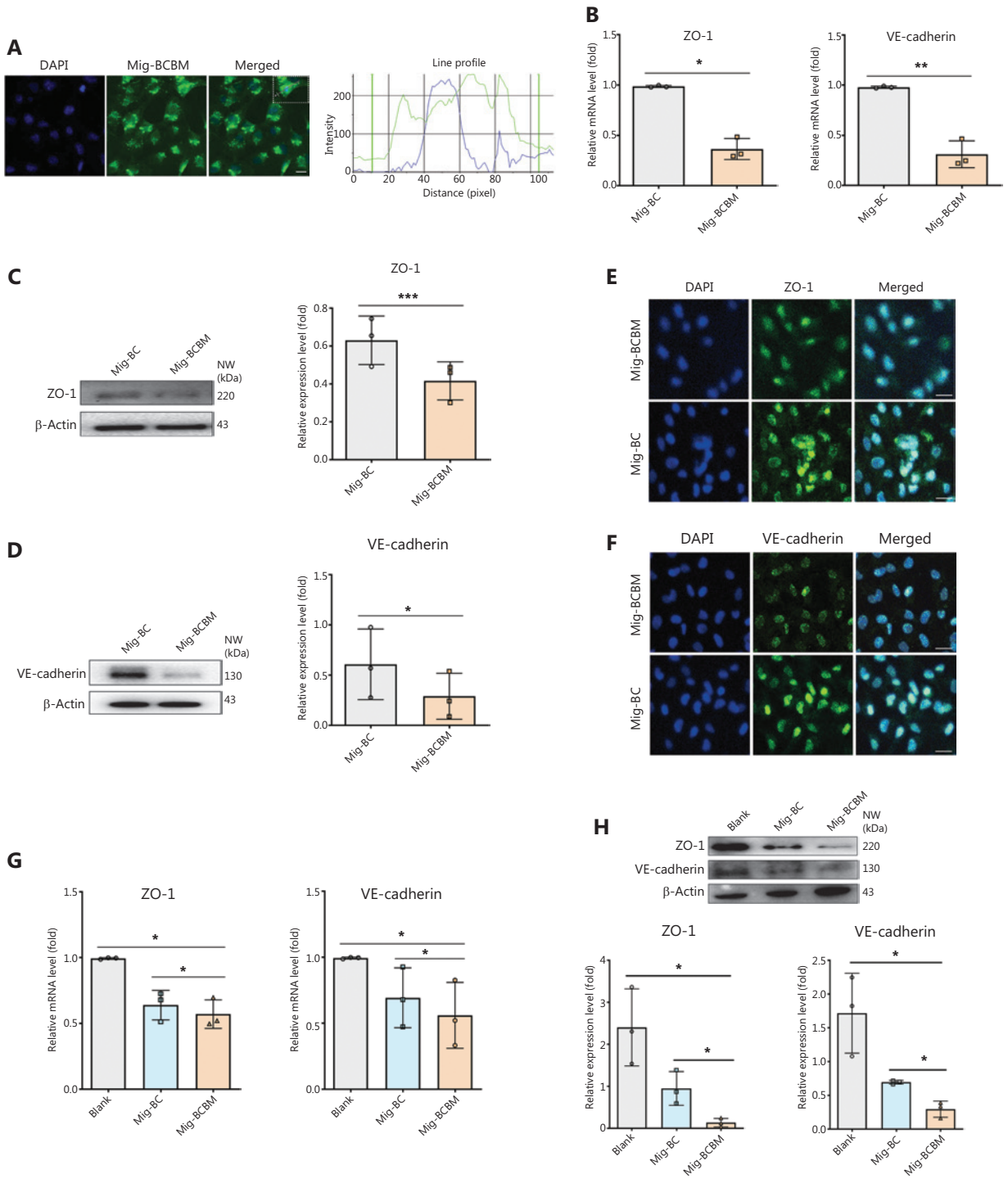


Figure 3 Mig-BCBM modulates BBB permeability by altering ZO-1 and VE-cadherin expression in hCMEC/D_3 cells. (A) Internalization of Mig-BCBM into hCMEC/D_3 cells. hCMEC/D_3 cells were incubated with WGA-labeled Mig-BCBM for 24 h. The right panel shows the line profile of representative cell images in the dashed box using Image-Pro Plus software. The right panel shows the line profile of the image of a representative cell within the dashed box, generated using the Image-Pro Plus software. The fluorescence images revealed efficient endocytosis of Mig-BCBM into hCMEC/D_3 cells. Scale bar, 10 μm. (B) Downregulation of *ZO-1* and *VE-cadherin* mRNA expression by Mig-BCBM. n = 3 (C and D) Decrease in ZO-1 (C) and VE-cadherin (D) protein expression following Mig-BCBM treatment. n = 3. (E and F) Effects of Mig-BCBM on the expression, but not subcellular localization, of *ZO-1* and *VE-cadherin*. Immunofluorescence staining revealed that Mig-BCBM treatment

reduced the levels of ZO-1 and VE-cadherin expression in hCMEC/D_3 cells without affecting the subcellular localization. Scale bar, 20 μm. (G and H) Effects of Mig-BCBM on *ZO-1* and *VE-cadherin* expression in mouse brains. Mig-BCBM (200 μg/mL) was injected into the mice brain. *ZO-1* and *VE-cadherin* mRNA (G) and protein (H) expression was downregulated. $n = 3$; *$P < 0.05$, **$P < 0.01$, ***$P < 0.001$.

A crucial event in brain metastasis involves the traversal of cancer cells across the BBB. Cerebral vascular endothelial cells have a pivotal role in determining BBB permeability[44]. First, an endothelial cell layer permeability test was performed to assess the effect of 231-BR cells-derived migrasomes on vascular endothelial barrier permeability. The hCMEC/D_3 cell layers were exposed to Mig-BCBM or Mig-BC for 48 h, followed by the addition of FITC-labled dextran (**Figure 1F**). Upon addition of dextran for 10, 20, 30, 40, and 50 min, the fluorescence intensity in the Mig-BCBM treatment group was significantly higher than the Mig-BC group (**Figure 1G**). The effect of Mig-BCBM on the metastatic capacity of 231-BR cells when traversing vascular endothelial barriers *in vitro* was then determined. The hCMEC/D_3 cell layers were treated with Mig-BCBM or Mig-BC for 48 h, then $^{GFP+}$231-BR cells were introduced and allowed to migrate for 12 h (**Figure 1H**). The number of $^{GFP+}$231-BR cells that traversed the hCMEC/D_3 cell layer in the Mig-BCBM group was significantly higher than the Mig-BC group (**Figure 1I and 1J**). Taken together, these findings suggest that Mig-BCBM effectively enhances the permeability of vascular endothelial layers and facilitates the metastasis of 231-BR cells across endothelial barriers *in vitro*.

Mig-BCBM enhances BBB permeability and promotes BCBM *in vivo*

Mig-BCBM was pre-injected into the tail veins of mice to evaluate the effect of 231-BR cells-derived migrasomes on BCBM, then the BCBM models were established by intracardiac injection of 231-BR cells (**Figure 2A**). Four weeks later, the brain tissues were collected and the brain metastases nodules were counted using H&E staining. As shown in **Figure 2B and 2C**, Mig-BCBM significantly enhanced brain metastases compared to the Mig-BC and control groups, with mean brain metastatic nodule counts of 23.6, 10.0, and 3.8, respectively. No detectable metastatic foci were observed in the liver and lungs (**Figure S1**). These data indicated that Mig-BCBM promotes BCBM *in vivo*.

Given that BBB maintains brain microenvironment homeostasis and restricts the entry of exogenous macromolecules and cells into the brain parenchyma, whether Mig-BCBM promotes BCBM *via* disrupting the BBB was determined. Mig-BCBM was pre-injected into the tail veins of mice. EB, a tracer for monitoring BBB disruption, was injected into the mice after 4 weeks (**Figure 2D**). Compared to the Mig-BC and control groups, EB-stained brain sections exhibited increased EB uptake in the Mig-BCBM-injected models (**Figure 2E**). Quantitative analysis of EB extravasation demonstrated significantly elevated cerebrovascular permeability in the Mig-BCBM group (8.729 μg/mL) compared to the control (6.772 μg/mL) and Mig-BC groups (7.857 μg/mL; **Figure 2F**). These results indicated that Mig-BCBM enhances BBB permeability *in vivo*.

Mig-BCBM internalizes into hCMEC/D_3 cells and downregulates t ZO-1 and VE-cadherin expression

Having determined that Mig-BCBM enhances the permeability of BBB *in vivo* and vascular endothelial layers *in vitro*, the impact on vascular endothelial cells was determined. First, it was imperative to ascertain whether Mig-BCBM could be transferred to hCMEC/D_3 cells. Recipient cells were incubated with WGA-labeled Mig-BCBM for 24 h. The results showed a large amount of Mig-BCBM internalized into hCMEC/D_3 cells (**Figure 3A**).

The hCMEC/D_3 cell tight junction protein, ZO-1, and adherens junction protein, VE-cadherin, have major roles in BBB integrity[25]. The effect of Mig-BCBM on the expression and subcellular localization of ZO-1 and VE-cadherin was further investigated. As shown in **Figure 3B-3F**, Mig-BCBM significantly decreased ZO-1 and VE-cadherin mRNA and protein expression in hCMEC/D_3 cells compared to the Mig-BC control group. However, Mig-BCBM did not alter the subcellular localization of ZO-1 and VE-cadherin within the recipient cells (**Figure 3E and 3F**).

To further validate these findings *in vivo*, ZO-1 and VE-cadherin expression in brain tissues of mice following the injection of Mig-BCBM was determined. ZO-1 and VE-cadherin mRNA and protein expression in brain tissues was downregulated after Mig-BCBM injection compared to Mig-BC and the blank control groups (**Figure 3G and 3H**), which was consistent with the *in vitro* data. Additionally,

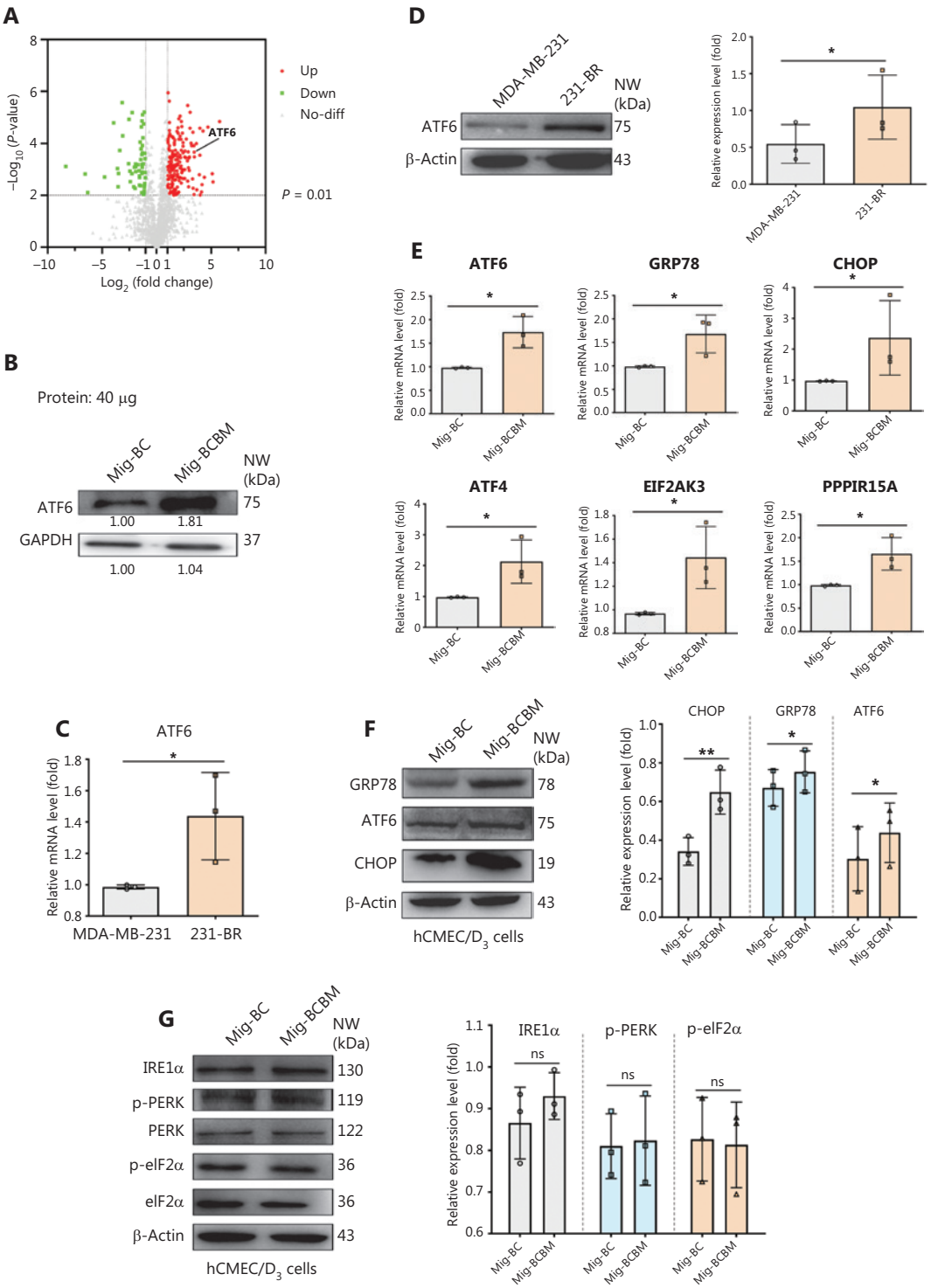


Figure 4 Mig-BCBM induces ER stress in hCMEC/D_3 cells. (A) Volcano plot depicting differential abundance proteins in Mig-BCBM compared to Mig-BC. Mig-BCBM and Mig-BC underwent 4D label-free quantitative mass spectrometry analysis. The red dots signify a Mig-BCBM/Mig-BC abundance ratio ≥ 2 (P < 0.01), while the green dots denote a Mig-BCBM/Mig-BC abundance ratio ≤ 0.5 (P < 0.01). n = 3 biologically independent experiments. (B) ATF6 expression in Mig-BCBM compared to Mig-BC. Mig-BCBM and Mig-BC were normalized with total protein and subjected to western blotting analysis. The gray values of the western blotting bands were quantified using ImageJ software. (C and D) Enhanced ATF6 expression in 231-BR cells. RT-qPCR (C) and western blotting (D) analyses revealed a significant upregulation of ATF6 in 231-BR

cells compared to MDA-MB-231 cells. *n* = 3. (E) Elevated expression of ER stress markers in hCMEC/D_3 cells treated with Mig-BCBM. RT-qPCR analyses revealed significant upregulation of six ER stress markers, including *ATF6*, *GRP78*, *CHOP*, *ATF4*, *EIF2AK3*, and *PPPIR15A*, in hCMEC/D_3 cells that had been exposed to Mig-BCBM. *n* = 3. (F) Enhanced protein expression of ER stress markers in Mig-BCBM-treated hCMEC/D_3 cells. Western blotting analyses confirmed the elevated protein levels of three ER stress markers (ATF6, GRP78, and CHOP) in hCMEC/D_3 cells that were subjected to treatment with Mig-BCBM. *n* = 3. (G) Protein expression of additional ER pathway markers (PERK and IRE1 pathways). Western blot analyses revealed no significant changes in p-PERK, p-eIF2α, or IRE1α in Mig-BCBM-treated hCMEC/D_3 cells compared to Mig-BC. *n* = 3; *P < 0.05, **P < 0.01; ns, no significance.

immunofluorescence staining confirmed that Mig-BCBM did not alter the membrane localization of ZO-1 and VE-cadherin in brain tissues (**Figure S2A and S2B**). Taken together, these data suggested that BCBM-derived migrasome Mig-BCBM increased BBB permeability by downregulation of vascular endothelial cell ZO-1 and VE-cadherin.

Mig-BCBM induces ER stress *via* ATF6 in hCMEC/D_3 cells

Having determined that Mig-BCBM promotes BBB permeability by downregulating ZO-1 and VE-cadherin, the underlying mechanism was clarified. 4D label-free proteomics analysis was performed on Mig-BCBM and Mig-BC. Quantitative mass spectrometry revealed differential protein enrichment between the two groups with ATF6 notably more abundant in Mig-BCBM compared to Mig-BC (**Figure 4A**). Western blotting analysis was performed to verify enrichment of ATF6 in Mig-BCBM. Consistent with the proteomics analysis results, ATF6 was significantly more abundant in Mig-BCBM compared to Mig-BC (**Figure 4B**). ATF6 expression in both cell lines was determined to ascertain whether enrichment of ATF6 in Mig-BCBM was due to differential expression between 231-BR and MDA-MB-231 cells. ATF6 was significantly upregulated in 231-BR cells compared to MDA-MB-231 cells (**Figure 4C and 4D**).

Significant enrichment of pathways related to the endoplasmic reticulum and Golgi vesicle-mediated transport and the UPR within Mig-BCBM was confirmed based on Gene Ontology (GO) analysis (**Figure S3**). Notably, ATF6 has emerged as a pivotal regulator of the UPR and has a crucial role in maintaining ER function and protein homeostasis[45]. Therefore, we postulated that entry of Mig-BCBM into hCMEC/D_3 cells may elicit ER stress in recipient cells. The mRNA levels of various ER stress markers, including *ATF6*, *GRP78*, *CHOP*, *ATF4*, *EIF2AK3*, and *PPPIR15A*, were all increased in Mig-BCBM-treated hCMEC/D_3 cells compared to the Mig-BC control group (**Figure 4E**). Upregulation of ATF6, GRP78, and CHOP protein expression further confirmed the ability of Mig-BCBM' to induce ER stress in hCMEC/D_3 cells (**Figure 4F**). Additional ER stress pathways were further examined by assessing p-PERK, p-eIF2α (PERK pathway), and IRE1α (IRE1 pathway). Mig-BCBM did not significantly alter activation of p-PERK, p-eIF2α, and IRE1α compared to Mig-BC (**Figure 4G**). These results suggested Mig-BCBM may induce ER stress of hCMEC/D_3 cells *via* the ATF6 pathway.

Expression of ER stress-related genes in brain tissues of mice following injection of Mig-BCBM was determined to further validate the capacity of Mig-BCBM to induce ER stress *in vivo*. The levels of ATF6, GRP78, and CHOP expression were significantly upregulated in the Mig-BCBM group compared to Mig-BC or PBS group mRNA and protein expression (**Figure 5A and 5B**). These findings confirmed that Mig-BCBM induces ER stress *in vivo*.

Mig-BCBM reverses the upregulation of ZO-1 and VE-cadherin caused by ATF6 knockdown in hCMEC/D_3 cells

ATF6 is transferred to the Golgi apparatus during ER stress, where ATF6 is cleaved by S1P and S2P proteases, and subsequently transferred to the nucleus to activate ER stress-related genes[45]. We hypothesized that the ATF6 pathway has an important role in downregulation of ZO-1 and VE-cadherin induced by Mig-BCBM; inhibiting this pathway might reverse the downregulation effect. Lentivirus was used to knockdown ATF6 expression in hCMEC/D_3 cells. As shown in **Figure 6A-C**, sh-ATF6 lentiviruses were successfully transduced into hCMEC/D_3 cells, resulting in a significant downregulation of ATF6 in mRNA and protein expression. Mig-BCBM was added after knocking down ATF6 in hCMEC/D3 cells. The levels of ZO-1 and VE-cadherin expression were upregulated after ATF6 knockdown in hCMEC/D_3 cells but this phenomenon was reversed after addition of Mig-BCBM (**Figure 6D**

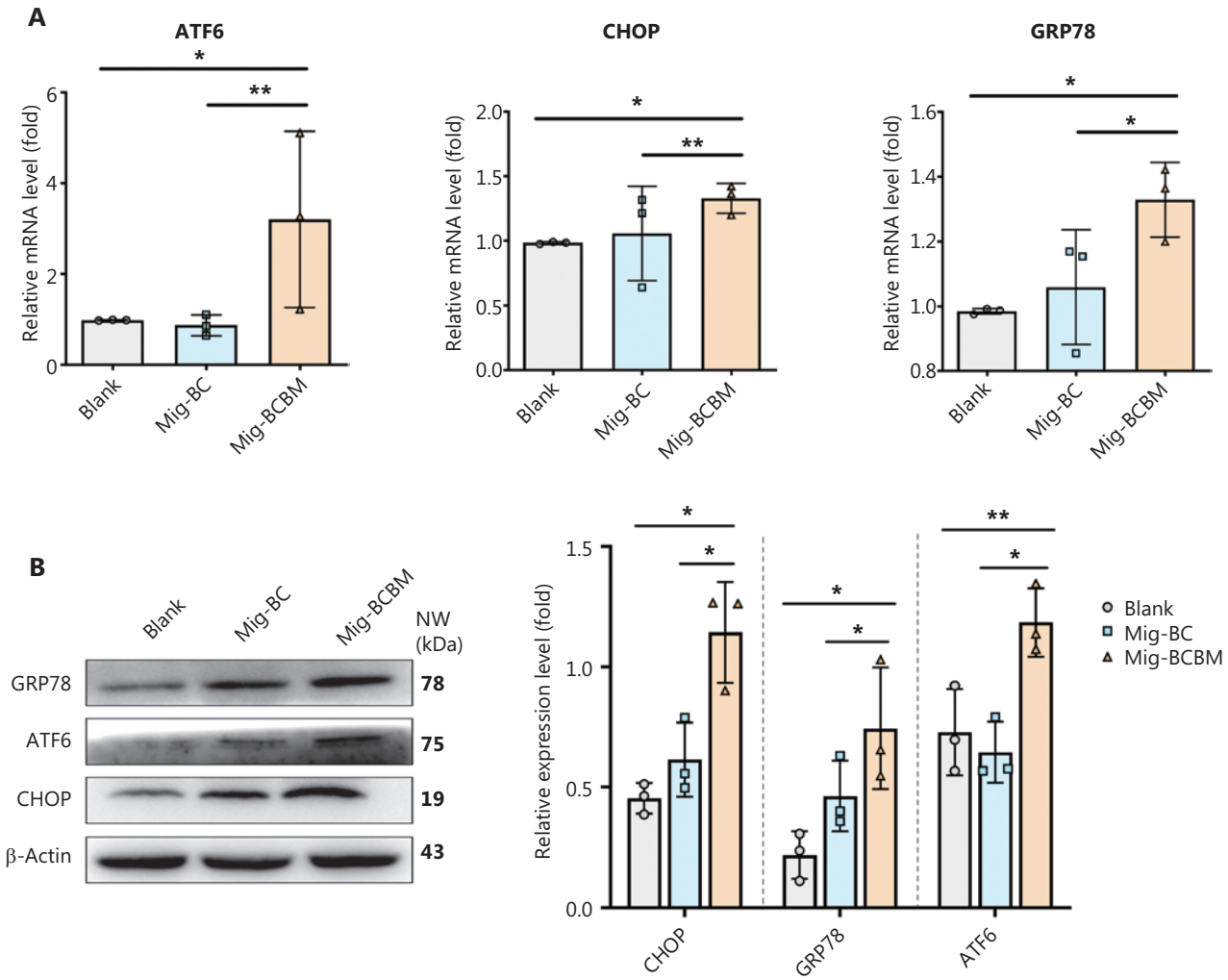


Figure 5 Mig-BCBM induces ER stress in mouse brains *in vivo*. (A) Elevated transcript levels of *GRP78*, *CHOP*, and *ATF6* in Mig-BCBM-exposed mouse brains. (B) Enhanced expression of GRP78, CHOP, and ATF6 protein in Mig-BCBM-treated mouse brains. *P < 0.05, **P < 0.01.

and 6E). Moreover, knockdown of ATF6 in hCMEC/D_3 cells led to suppression of the metastatic potential of 231-BR cells traversing vascular endothelial barriers. However, the addition of Mig-BCBM into hCMEC/D_3 cells reversed this inhibitory effect (**Figure 6F**). These findings indicated that ATF6 knockdown elevates the expression of ZO-1 and VE-cadherin in hCMEC/D_3 cells, whereas Mig-BCBM reverses this upregulation.

ATF6 was knocked down in Mig-BCBM (Mig-shATF6) to further investigate the functional role of ATF6 in migrasome-mediated BBB disruption and 231-BR cell transendothelial migration (**Figure 6G**). Quantitative analysis revealed that ATF6 depletion significantly reduces BBB permeability compared to the Mig-shNC control, as demonstrated by decreased dextran fluorescence intensity across all time points (10–50 min; **Figure 6H**). Furthermore, transendothelial migration assays using GFP-labeled 231-BR cells showed a marked reduction in cell penetration through hCMEC/D_3 monolayers in the Mig-shATF6 group *vs.* Mig-shNC (**Figure 6I**). These findings suggested that ATF6 is a critical mediator in migrasomes by regulating BBB integrity and metastatic cell transmigration, and thereby influencing final metastatic outcomes.

Mig-BCBM promotes BCBM by triggering ER stress in hCMEC/D_3 cells

Cells were pretreated with ER stress inhibitors (4-PBA), followed by Mig-BCBM exposure for 48 h, then ER stress markers

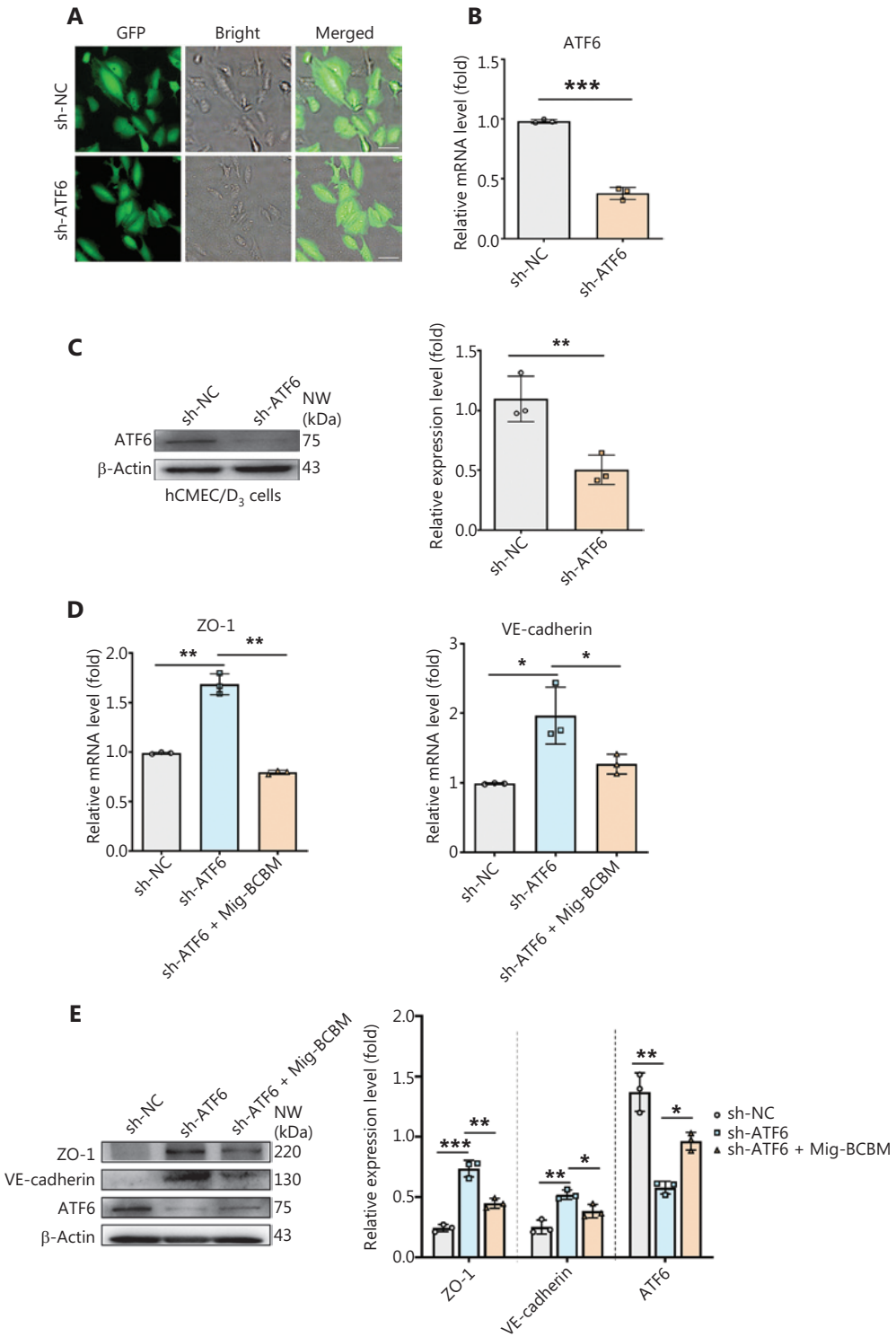


Figure 6 Continued

expression was determined to further clarify the Mig-BCBM' induction effect on ER stress in hCMEC/D_3 cells. As shown in **Figure 7A**, upon pretreatment with 4-PBA, the levels of CHOP, GRP78, and ATF6 expression in hCMEC/D_3 cells were suppressed, but Mig-BCBM significantly attenuated downregulation of these molecules caused by 4-PBA. Moreover, 4-PBA

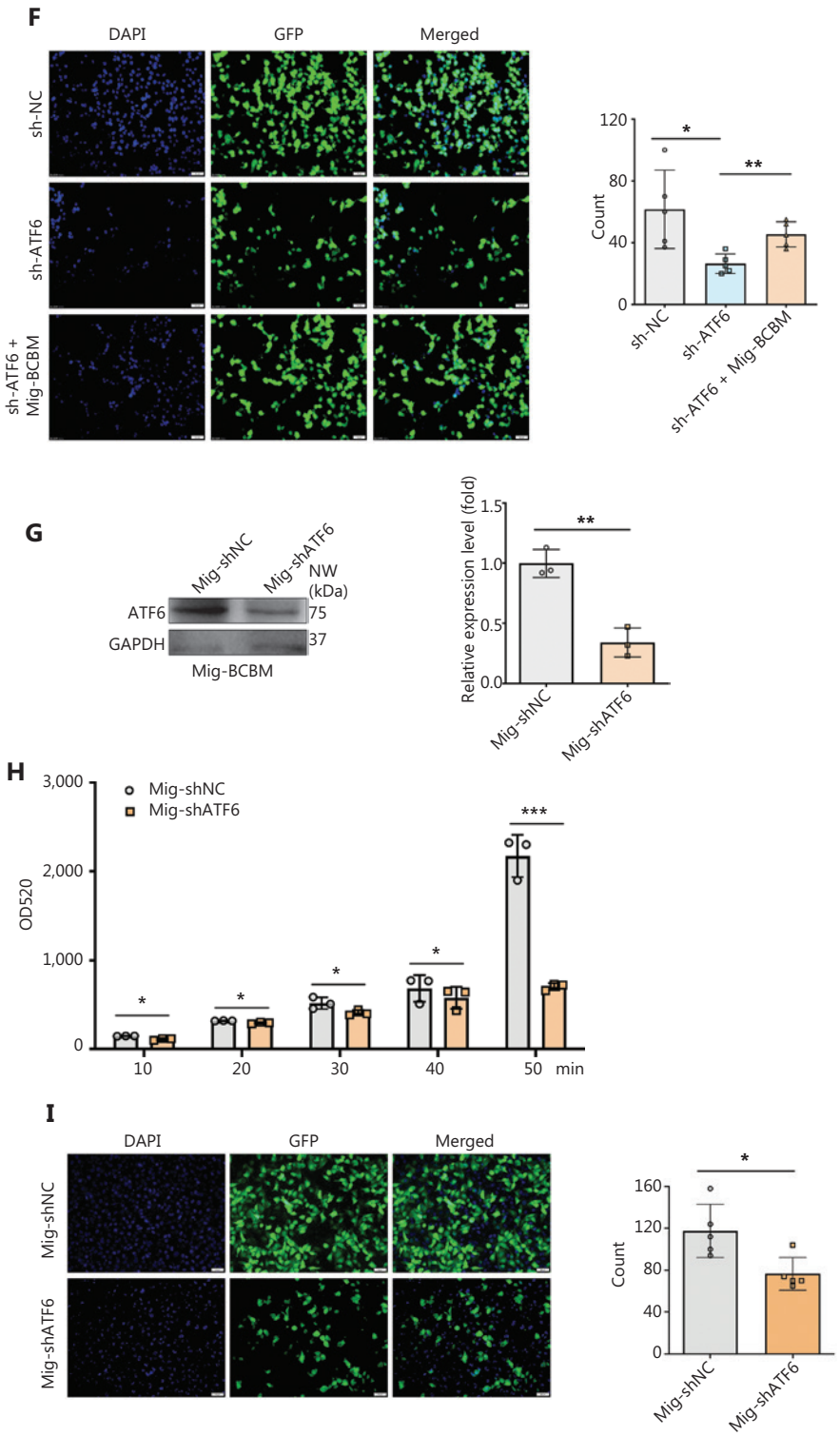


Figure 6 Mig-BCBM reverses ZO-1 and VE-cadherin upregulation induced by ATF6 knockdown in hCMEC/D_3 cells. (A–C) Efficient knockdown of ATF6 in hCMEC/D_3 cells. The knockdown efficiency of ATF6 in hCMEC/D_3 cells was examined using immunofluorescent staining (A), RT-qPCR (B), and western blotting (C). Scale bars, 50 μm; n = 3. (D–E) ATF6 knockdown upregulates ZO-1 and VE-cadherin expression, which is reversed by Mig-BCBM. The mRNA (D) and protein (E) levels were upregulated after ATF6 knockdown in hCMEC/D_3 cells, but this phenomenon was reversed after the addition of Mig-BCBM. n = 3. (F) ATF6 knockdown inhibits the metastatic potential of 231-BR cells traversing vascular

endothelial barriers, but this phenomenon was reversed after the addition of Mig-BCBM. Scale bars, 50 μm; *n* = 5. (G) Efficient knockdown of ATF6 in Mig-BCBM (Mig-shATF6). *n* = 3. (H) Effect of Mig-shATF6 on hCMEC/D_3 cell layer permeability. *n* = 3. (I) Scale bars, 50 μm. Effect of Mig-shATF6 on the migration of 231-BR cells across vascular endothelial layers. Quantification of $^{GFP+}$231-BR cell migration through vascular endothelial layers. *n* = 5; **P* < 0.05, ***P* < 0.01, ****P* < 0.001.

led to upregulation of ZO-1 and VE-cadherin in hCMEC/D_3 cells but this effect was reversed upon addition of Mig-BCBM (**Figure 7B**).

Rescue experiments were performed to further validate the effect of Mig-BCBM on ZO-1 and VE-cadherin expression through induction of ER stress *in vivo*. The mice were initially injected with Mig-BCBM *via* the tail veins and after a 2-h interval 4-PBA was administered intraperitoneally. 4-PBA reversed Mig-BCBM-induced downregulation of ZO-1 and VE-cadherin (**Figure 7C**).

In vivo rescue experiments were performed to further confirm the mechanism underlying Mig-BCBM in enhancing brain metastases *via* induction of ER stress. The mice were injected intraperitoneally with 4-PBA and 2 h later Mig-BCBM was administered *via* the tail veins. This injection schedule was repeated twice weekly for a total of 4 weeks. The BCBM models were established by injecting $^{GFP+}$231-BR cells into the left ventricles (**Figure 7D**). Whole-brain *ex vivo* fluorescence imaging revealed that Mig-BCBM facilitates the development of brain metastases, whereas 4-PBA effectively mitigates the brain metastases triggered by Mig-BCBM (**Figure 7E and 7F**).

ATF6 expression in human serum migrasomes as a potential molecular marker for diagnosing BCBM

Having confirmed that Mig-BCBM downregulates ZO-1 and VE-cadherin expression in hCMEC/D_3 cells *via* the release of ATF6 resulting in BBB impairment and ultimately facilitating the process of BCBM, the association between the levels of ATF6 in human serum migrasomes and BCBM

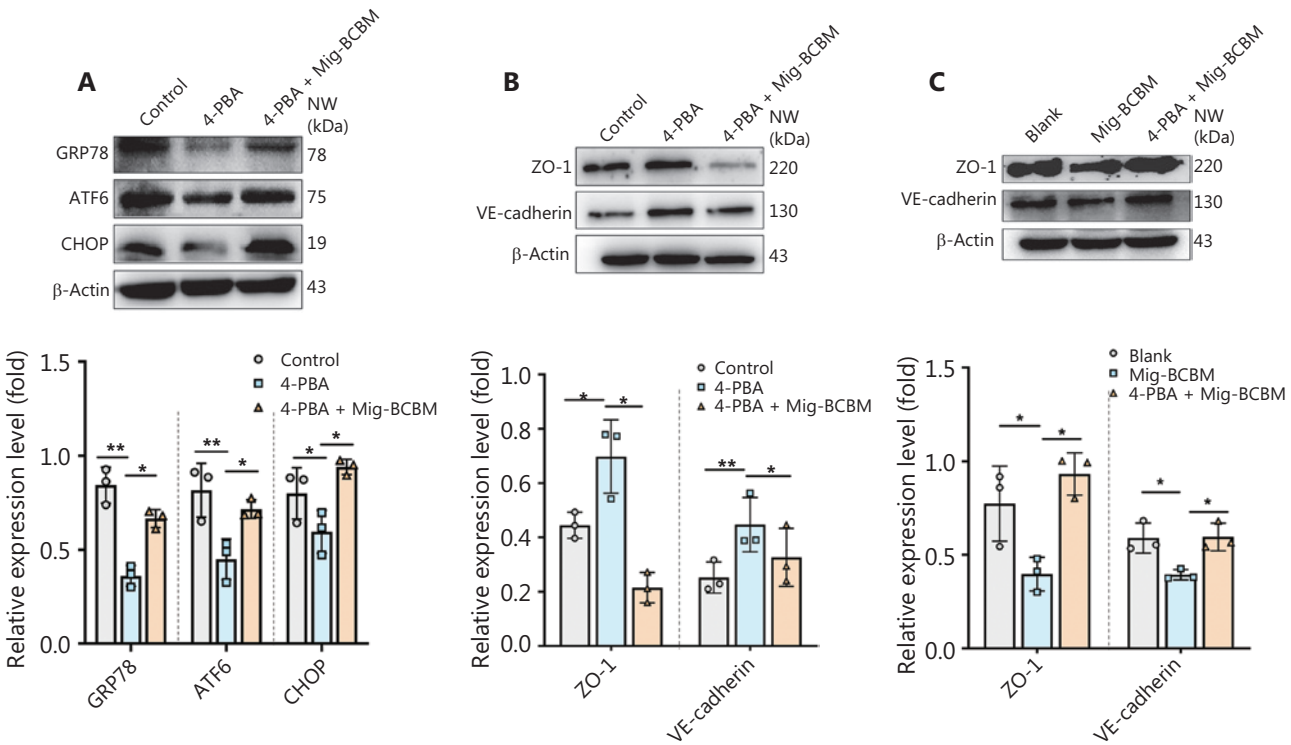


Figure 7 Continued

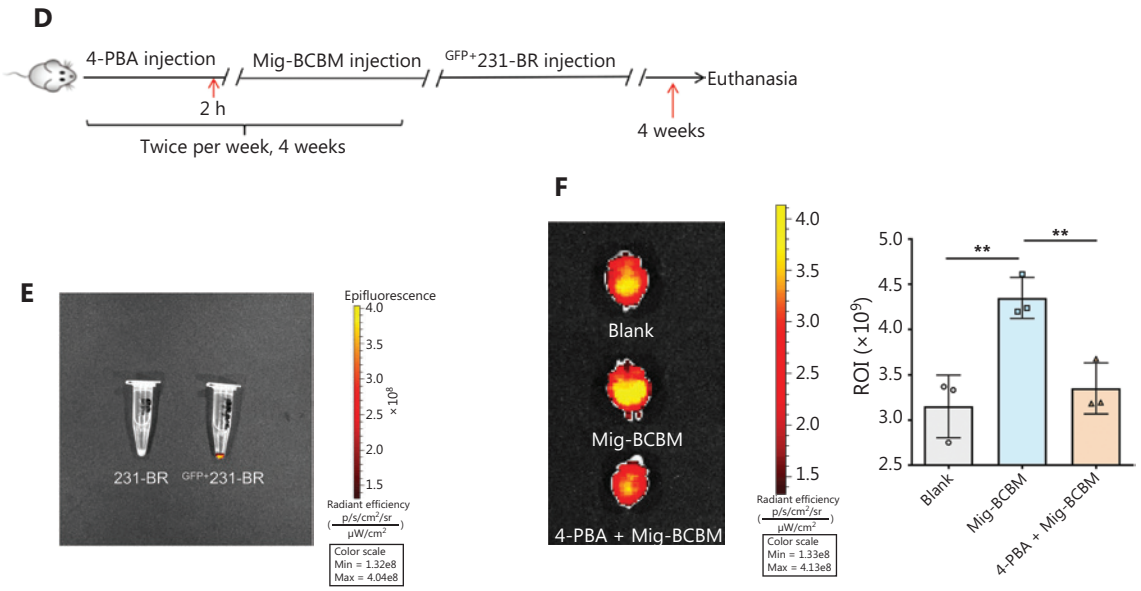


Figure 7 Mig-BCBM enhances BCBM *via* the induction of ER stress. (A) Mig-BCBM rescued the downregulation of CHOP, GRP78, and ATF6 caused by 4-PBA in hCMEC/D_3 cells. n = 3. (B) Mig-BCBM rescued the upregulation of ZO-1 and VE-cadherin caused by 4-PBA in hCMEC/D_3 cells. n = 3. (C) 4-PBA reversed the Mig-BCBM-induced downregulation of ZO-1 and VE-cadherin *in vivo*. n = 3. (D) Schematic illustration of an *in vivo* rescue experiment to confirm the role of Mig-BCBM in enhancing BCBM through ER stress. The mice were intraperitoneally injected with 4-PBA, followed by the administration of Mig-BCBM through the tail vein 2 h later. The mice underwent a twice-weekly injection schedule for 4 weeks. The BCBM models were established by injecting $^{GFP+}$231-BR cells into the left ventricle. (E–F) 4-PBA reduced the brain metastases caused by Mig-BCBM *in vivo*. Fluorescence images of $^{GFP+}$231-BR cells (E). Whole-brain *ex vivo* fluorescence images and ROI value of fluorescence intensity of mouse metastases (F). n = 3; *P < 0.05, **P < 0.01.

were determined. First, serum samples were collected from patients with BCBM and primary BC, and healthy individuals. The serum migrasomes were purified using a density gradient centrifugation technique (**Figure 8A**). The SEM and TEM images clearly demonstrated that the majority of serum migrasomes exhibited a round or nearly round morphology enveloped by membranes (**Figure 8B and 8C**). Furthermore, western blotting analysis revealed the presence of NDST1, CPQ, and PIGK in the serum migrasomes (**Figure 8D**), confirming successful isolation from serum migrasome samples.

Western blotting analysis was performed to determine the association between the levels of ATF6 protein in human serum migrasomes and BCBM. The findings revealed significantly elevated levels of ATF6 in the serum migrasome samples of BCBM patients in contrast to the levels of ATF6 in BC patients and healthy controls (**Figure 8E**). Given the limitations of western blotting in clinical molecular diagnosis, dPCR experiments were performed to further assess the diagnostic potential of *ATF6* levels in serum migrasomes. Interestingly, *ATF6* was detected in the serum migrasomes of BCBM and BC patients, and healthy controls. Importantly, a significant increase in *ATF6* expression was noted in the serum migrasome samples of patients with BCBM compared to BC and healthy controls (**Figure 8F and 8G**), suggesting that detection of *ATF6* expression in human serum migrasomes may potentially serve as a molecular marker for diagnosing BCBM.

Discussion

This is the first report that investigated the function and plausible molecular mechanism underlying cancer-derived migrasomes in tumor metastasis, specifically in the context of BCBM. Although there has been some progress in determining the mechanisms underlying BCBM, the exact molecular mechanisms have not been established. A novel mechanism in which cancer-derived migrasome Mig-BCBM, acting as novel EVs, disrupt BBB integrity and consequently promote the progression of BCBM was elucidated in the current study.

Mig-BCBM suppressed ZO-1 and VE-cadherin expression in hCMEC/D_3 cells by inducing ER stress through the delivery of ATF6. These findings enhance our understanding of the complex mechanisms underlying BCBM and highlight the crucial role of Mig-BCBM in compromising BBB integrity. Indeed, the current study findings have contributed significantly to the expanding knowledge base of cancer-derived migrasomes and offer promising avenues for potential therapeutic strategies in the treatment of BCBM.

Migrasomes belong to a novel class of EVs that have aroused considerable research interests[46]. Currently, most research is directed towards elucidating the fundamental biology of migrasomes, encompassing the discovery, generation, characteristics, and functions[47]. The role of migrasomes in pathophysiologic processes remains to be definitively determined. Given that migrasomes are generated during cell migration, cancer cells, which exhibit highly active migratory behaviors, are likely to produce a substantial quantity of migrasomes during the migration process. We hypothesized that these cancer-derived migrasomes may have a pivotal role in tumor metastasis. Our data indicated that 231-BR cell-derived migrasome Mig-BCBM effectively enhance the permeability of vascular endothelial layers and facilitate 231-BR cell metastasis across endothelial barriers *in vitro*. Moreover, Mig-BCBM was shown to augment BBB permeability and promote BCBM in BCBM models. The findings revealed that Mig-BCBM may serve as a mediator of long-distance signaling delivery between cancer cells and cerebral vascular endothelial cells, effectively disrupting the integrity of BBB and thereby promoting the formation of PMN in the brain, which ultimately facilitates the occurrence of BCBM. Apart from vascular endothelial cells, parenchymal basement membranes, pericytes and astrocyte foot processes (end-feet) also provide barrier function[22]. Further investigations are still warranted to elucidate whether Mig-BCBM impacts BBB permeability by influencing these specific cell types.

Previous research has demonstrated that migrasomes have an important role in maintaining mitochondrial quality in migrating cells[48]. This finding suggested that cancer cell-derived migrasomes may release harmful cellular components that damage the integrity of BBB. Tumor cells usually proliferate vigorously with exuberant metabolism and encounter a harsh surviving environment, such as nutrient deficiency, oxygen shortage, and oxidative stress, which could trigger ER stress[49]. In stress-free ER, GRP78 binds to and blocks the function of ER stress sensors (ATF6, IRE1, and PERK). The accumulated misfolded or unfolded proteins recruit GRP78 away from sensors during ER stress, which would consequently activate UPR and initiate adaptive responses that promote ER stress-related gene expression to orchestrate recuperation of ER function[50]. In the current study, the presence of ATF6 in Mig-BCBM was demonstrated. Upon treatment with Mig-BCBM, ER stress-related factors, such as ATF6, GRP78, ATF4, EIF2AK3, PPPIR15A, and CHOP, were all significantly upregulated in hCMEC/D_3 cells, suggesting a boosted ER stress. In addition to ATF6, the IRE1 and PERK pathways were evaluated. Mig-BCBM did not significantly activate IRE1α, p-PERK, or p-eIF2α compared to Mig-BC. Mig-BCBM elicited ER stress in hCMEC/D_3 cells through the delivery of ATF6, highlighting the intricate and complex interplay between Mig-BCBM and cellular stress responses.

Proteomic analysis revealed that expression of high-mobility group box 1 (HMGB1) and S100A10, in addition to ATF6, were also significantly altered in Mig-BCBM compared to Mig-BC. HMGB1, a nuclear protein with multiple functions outside cells, is involved in activating the innate immune system and regulating autophagy, cytokine release, angiogenesis, and tumor cell proliferation and migration[51]. The role of HMGB1 in LPS-induced neuroinflammation and damage to the BBB further underscores the relevance of HMBG1[52]. Studies have shown that HMGB1 upregulation in BC cells affect the tumor microenvironment, promoting migration and invasion[53]. S100A10 is a multifunctional protein with a wide range of physiologic activity[54]. S100A10 promotes immune microenvironment remodeling by recruiting myeloid-derived suppressor cells[55] and accelerates cancer progression through extracellular vesicle-mediated protein cargo regulation[56]. While HMGB1/S100A10 showed significant changes, ATF6 was selected as the mechanistic focus due to its direct role in ER stress-mediated BBB dysfunction and established relevance to BCBM progression. Additional proteins with potential roles in BBB permeability or the tumor microenvironment will be systematically investigated in corollary studies.

Tight and adherens junctions between cerebrovascular endothelial cells are the major determinants of BBB integrity[57,58]. ZO-1 and VE-cadherin are two indispensable components in maintenance of BBB integrity. ZO-1 and VE-cadherin expression were reduced in Mig-BCBM-treated hCMEC/D_3 cells without any alteration in the subcellular localization. 4-PBA rescue assays demonstrated that downregulation of ZO-1 and VE-cadherin expression in hCMEC/D_3 cells was indeed mediated by elicitation of ER stress through ATF6.

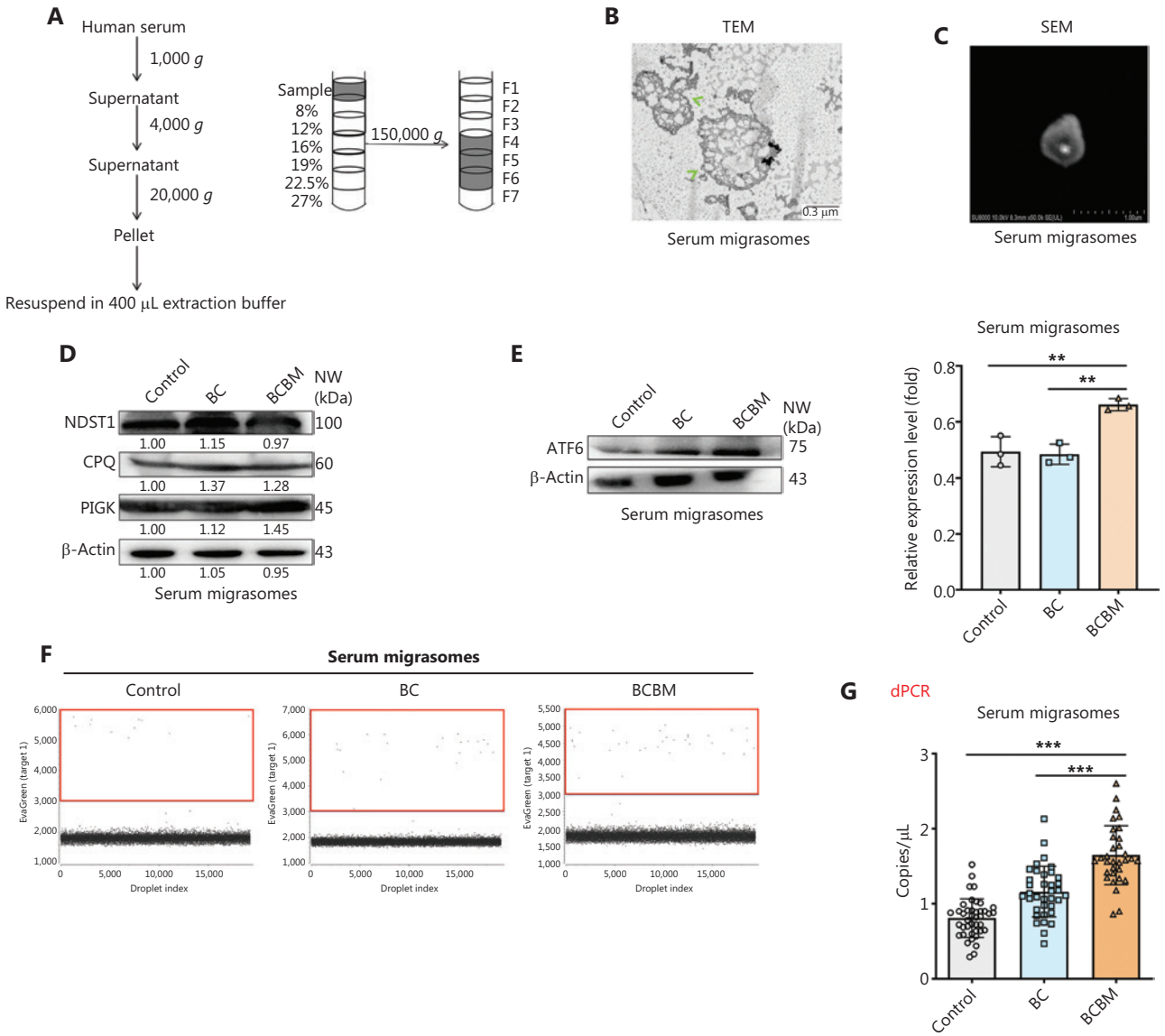


Figure 8 Expression of ATF6 in serum migrasomes of BCBM patients. (A) Flowchart of isolation and purification of serum migrasomes. (B–D) Identification and characterization of serum migrasomes. The human serum migrasomes were identified using TEM (B), SEM (C), and western blotting (D). The green arrows indicate migrasomes in (B). Scale bars, 0.3 μm in (B) and 1 μm in (C). (E) Elevated protein levels of ATF6 in serum migrasome samples of BCBM patients compared to BC patients and healthy controls. n = 3. (F and G) Evaluation of *ATF6* mRNA expression in serum migrasomes utilizing digital PCR (dPCR). Representative imaging obtained from the dPCR analysis of *ATF6* mRNA expression within serum migrasomes (F) and quantitative analysis (G). BCBM, n = 32; BC, n = 36; control, n = 41; $^{**}P < 0.01$, $^{***}P < 0.001$.

Given these discoveries, we propose that blocking the formation of cancer-derived migrasomes or inhibiting the expression of ATF6 within migrasomes may represent a novel strategy for the early intervention of BCBM. 4-PBA, a histone deacetylase (HDAC) and ER stress inhibitor, has been shown to be safe at various doses with no significant impact on cell proliferation or apoptosis in different models and no observed organ damage in animal studies[59,60]. 4-PBA protects cardiomyocytes and vascular endothelial cells by reducing ER stress, mitigating cardiac rupture, and post-infarction remodeling[61,62]. While this study focused on mechanistic exploration, future preclinical research, including large animal models and long-term toxicity experiments, will be essential to advance the translational application of 4-PBA.

EVs carry proteins and nucleic acids derived from the originating cells, making EVs viable candidates for the early

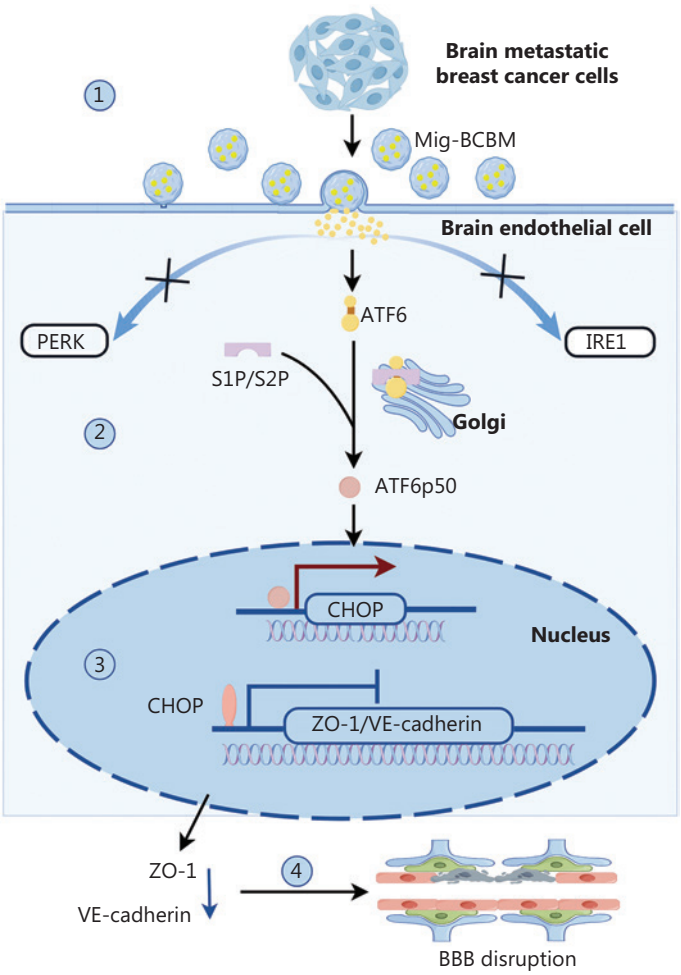


Figure 9 Schematic diagram of the proposed mechanism of Mig-BCBM in BBB disruption. Step-by-step mechanism: ① Mig-BCBM, derived from brain metastatic breast cancer cells, enters the brain microvasculature *via* the bloodstream. ② The Mig-BCBM migrasome membrane, enriched in cholesterol, sphingomyelin, and tetraspanins (e.g., TSPAN4), may form liquid-ordered lipid raft microdomains. These structural features enhance membrane fluidity, facilitating fusion with brain endothelial cells and subsequent cargo release. Mig-BCBM cargo contains ATF6 but lacks PERK and IRE1 pathway components. ATF6, a key ER stress sensor and transcription factor, translocates to the Golgi apparatus upon ER stress. Golgi-resident zinc metalloproteinases S1P/S2P sequentially cleave ATF6 to release the active fragment, ATF6p50. ③ ATF6p50 enters the nucleus, binds to the CHOP promoter, and upregulates CHOP expression. As an ER stress-inducible transcription factor, CHOP may bind to the promoter regions of ZO-1 and VE-cadherin, suppressing transcriptional activity. ④ Downregulation of ZO-1 and VE-cadherin disrupts tight junctions and adherens junctions, leading to BBB leakage. This compromised barrier facilitates the transendothelial migration of brain metastatic breast cancer cells. ER, endoplasmic reticulum; ATF6, activating transcription factor-6; PERK, protein kinase RNA-like endoplasmic reticulum kinase; IRE1, inositol-requiring enzyme 1; S1P/S2P, site-1 protease/site-2 protease; CHOP, C/EBP-homologous protein; ZO-1, zonula occludens 1; BBB, blood-brain barrier.

diagnosis of numerous diseases[63-65]. Migrasomes can also transport cytosolic contents, rendering EVs as valuable biomarkers for the detection of diseases. For example, podocyte injury results in the formation of migrasomes and the number of migrasomes in urine serves as a biomarker for the early diagnosis of podocyte injury[11,43]. To date, there is only one report that has demonstrated the presence of migrasomes in human serum[38]. However, it remains unclear whether serum migrasomes are associated with specific diseases, including tumors. Western blotting analysis revealed a significant upregulation of ATF6 protein expression in human serum migrasomes of BCBM patients in contrast to the relatively lower levels observed in BC patients and healthy controls. Notably, we identified β-actin in serum-derived migrasomes,

which is particularly interesting given that β-actin is typically undetectable in whole serum. This observation suggests that β-actin becomes enriched during the migrasome isolation process. The apparent absence of β-actin in whole serum can be attributed to the relatively low abundance of migrasomes in plasma. Due to the sensitivity limitations of western blotting we also performed dPCR experiments to assess the diagnostic potential of *ATF6* levels in serum migrasomes. dPCR is founded on the principle of partitioning reagents to a degree where single template molecules are amplified and visualized individually. This approach offers superior precision compared to traditional PCR techniques. dPCR is particularly well-suited for precision medicine applications that require accurate molecular characterization with high sensitivity[66-68]. Our findings demonstrated significant upregulation of ATF6 in the serum migrasome samples of patients with BCBM compared to patients with BC and healthy control subjects, which provided compelling evidence for the potential of ATF6 in human serum migrasomes as a novel diagnostic biomarker for BCBM. Further validation in an independent cohort with the integration of ATF6 and complementary biomarkers, such as NDST1, CPQ, and PIGK, could significantly enhance diagnostic accuracy. The current methodology presents practical limitations in clinical settings due to the technical challenges associated with migrasome isolation from serum, particularly the constraints of limited sample volumes and the complexity of sucrose density gradient centrifugation and ultracentrifugation. To address these limitations, we propose future optimizations, such as preliminary migrasome enrichment to streamline processing and the integration of advanced detection technologies like mass cytometry or dPCR to enhance sensitivity and reliability. These refinements could significantly improve the practicality and clinical applicability of serum migrasome analysis, paving the way for broader use in disease diagnosis and monitoring.

In the current study the MDA-MB-231/231-BR model was used as a tool to delve into the functions of migrasomes in the context of brain metastasis. However, cross-validation in additional models, such as HCC1954/HCC1954-Br and BT474/BT474-Br, remains essential to ensure biological generalizability. Future work will systematically evaluate migrasome roles across molecular subtypes to determine whether these mechanisms are universally conserved or subtype-dependent. The lack of hepatic and pulmonary metastases in the BCBM model reflects the intrinsic brain tropism of 231-BR cells, confirming migrasome-mediated brain metastasis while limiting assessment of systemic metastatic potential. To resolve whether this organ restriction arises from cellular tropism or migrasome functional constraints, future studies should use multimodal delivery routes (e.g., tail vein and intracardiac co-injection) with non-brain-tropic cell lines. Such systematic comparisons across organ systems will clarify the spatial regulatory logic of migrasome-mediated metastasis. While the current study demonstrated migrasome-mediated brain metastasis, direct comparisons between primary and metastatic sites are limited. Our plasma migrasome analysis revealed elevated ATF6 in brain metastasis patients, suggesting migrasome involvement in metastatic progression. Future studies will address tissue-level heterogeneity, as follows: (1) prospective collection of matched primary tumors and brain metastases; and (2) orthotopic mammary fat pad models to compare migrasome profiles between primary and metastatic sites. These investigations will clarify whether migrasome alterations represent drivers or bystanders of metastasis, while providing insight into the spatial regulation of migrasome biology during metastatic dissemination.

Conclusions

In conclusion, the current study revealed that cancer cell-derived migrasome Mig-BCBM disrupts the BBB and promotes the development of BCBM. Mechanistically, Mig-BCBM suppressed ZO-1 and VE-cadherin expression in hCMEC/D_3 cells by inducing ER stress *via* the delivery of ATF6 (**Figure 9**). These findings offer a novel understanding of migrasome-mediated signaling transduction and the contribution to BCBM, providing innovative candidate targets for the diagnosis and therapy of BCBM.

Grant support

This work was supported by the National Natural Science Foundation of China (Grant No. 81702884), Natural Science Foundation of Shandong Province (Grant Nos. ZR2022MH272, ZR2020QH216, and ZR2023QH115), and Medicine and Health Science and Technology Foundation of Shandong Province (Grant Nos. 202402060623 and 202202080721).

Conflict of interest statement

No potential conflicts of interest are disclosed.

Author contributions

Conceived and designed the analysis: Bo Fu, Wei Zhang, Meng An.
Collected the data: Song Wang, Guohao Gu, Xinmiao Xian, Jun Li, Di Zhang, Jianran Guo, Dong Yan Contributed data or analysis tools: Song Wang, Guohao Gu, Xinmiao Xian, Jun Li, Di Zhang, Jianran Guo, Anqi Zhang, Shen Chen, Dong Yan, Bingwu Yang.
Performed the analysis: Song Wang, Guohao Gu, Xinmiao Xian.
Wrote the paper: Song Wang, Bo Fu, Anqi Zhang

Data availability statement

The data generated in this study are available upon request from the corresponding authors.

References

1. Harbeck N, Penault-Llorca F, Cortes J, Gnant M, Houssami N, Poortmans P, et al. Breast cancer. Nat Rev Dis Primers. 2019; 5: 66.
2. Sun H, Xu J, Dai S, Ma Y, Sun T. Breast cancer brain metastasis: current evidence and future directions. Cancer Med. 2023; 12: 1007-24.
3. Aizer AA, Lamba N, Ahluwalia MS, Aldape K, Boire A, Brastianos PK, et al. Brain metastases: a Society for Neuro-Oncology (SNO) consensus review on current management and future directions. Neuro Oncol. 2022; 24: 1613-46.
4. Giordano G, Griguolo G, Landriscina M, Meattini I, Carbone F, Leone A, et al. Multidisciplinary management of HER2-positive breast cancer with brain metastases: an evidence-based pragmatic approach moving from pathophysiology to clinical data. Crit Rev Oncol Hematol. 2023; 192: 104185.
5. Mu R, Sun H, Zeng Y, Tong Y, Tang P, Zhao M, et al. Nanomodulators targeting endothelial WNT and pericytes to reversibly open the blood-tumor barrier for boosted brain tumor therapy. J Control Release. 2024; 369: 458-74.
6. Liu Z, Chen J, Ren Y, Liu S, Ba Y, Zuo A, et al. Multi-stage mechanisms of tumor metastasis and therapeutic strategies. Signal Transduct Target Ther. 2024; 9: 270.
7. Wang Y, Jia J, Wang F, Fang Y, Yang Y, Zhou Q, et al. Pre-metastatic niche: formation, characteristics and therapeutic implication. Signal Transduct Target Ther. 2024; 9: 236.
8. Ma L, Li Y, Peng J, Wu D, Zhao X, Cui Y, et al. Discovery of the migrasome, an organelle mediating release of cytoplasmic contents during cell migration. Cell Res. 2015; 25: 24-38.
9. Jiang D, He J, Yu L. The migrasome, an organelle for cell-cell communication. Trends Cell Biol. 2025; 35: 205-16.
10. Wang D, Yu L. Migrasome biogenesis: when biochemistry meets biophysics on membranes. Trends Biochem Sci. 2024; 49: 829-40.
11. Liu Y, Li S, Rong W, Zeng C, Zhu X, Chen Q, et al. Podocyte-released migrasomes in urine serve as an indicator for early podocyte injury. Kidney Dis (Basel). 2020; 6: 422-33.
12. Huang Y, Zucker B, Zhang S, Elias S, Zhu Y, Chen H, et al. Migrasome formation is mediated by assembly of micron-scale tetraspanin macrodomains. Nat Cell Biol. 2019; 21: 991-1002.
13. Zhu M, Zou Q, Huang R, Li Y, Xing X, Fang J, et al. Lateral transfer of mRNA and protein by migrasomes modifies the recipient cells. Cell Res. 2021; 31: 237-40.
14. Wang L, Zhu Y, Zhang L, Guo L, Wang X, Pan Z, et al. Mechanisms of PANoptosis and relevant small-molecule compounds for fighting diseases. Cell Death Dis. 2023; 14: 851.
15. Zhang K, Zhu Z, Jia R, Wang NA, Shi M, Wang Y, et al. CD151-enriched migrasomes mediate hepatocellular carcinoma invasion by conditioning cancer cells and promoting angiogenesis. J Exp Clin Cancer Res. 2024; 43: 160.
16. Zhang R, Peng J, Zhang Y, Zheng K, Chen Y, Liu L, et al. Pancreatic cancer cell-derived migrasomes promote cancer progression by fostering an immunosuppressive tumor microenvironment. Cancer Lett. 2024; 605: 217289.
17. Wang M, Xiong C, Mercurio AM. PD-LI promotes rear retraction during persistent cell migration by altering integrin β4 dynamics. J Cell Biol. 2022; 221: e202108083.
18. Geissler M, Jia W, Kiraz EN, Kulacz I, Liu X, Rombach A, et al. The brain pre-metastatic niche: biological and technical advancements. Int J Mol Sci. 2023; 24: 10055.
19. Carvalho R, Paredes J, Ribeiro AS. Impact of breast cancer cells′ secretome on the brain metastatic niche remodeling. Semin Cancer Biol. 2020; 60: 294-301.
20. Zhou M, Chen H, Zeng Y, Lv Z, Hu X, Tong Y, et al. DH5α outer membrane-coated biomimetic nanocapsules deliver drugs to brain metastases but not normal brain cells via targeting GRP94. Small. 2023; 19: e2300403.
21. Di Lorenzo R, Ahluwalia MS. Targeted therapy of brain metastases: latest evidence and clinical implications. Ther Adv Med Oncol. 2017; 9: 781-96.
22. Steeg PS. The blood-tumour barrier in cancer biology and therapy. Nat Rev Clin Oncol. 2021; 18: 696-714.
23. Arvanitis CD, Ferraro GB, Jain RK. The blood-brain barrier and blood-tumour barrier in brain tumours and metastases. Nat Rev Cancer. 2020; 20: 26-41.
24. Zhang T, Xu Z, Wen L, Lei D, Li S, Wang J, et al. Cadmium-induced dysfunction of the blood-brain barrier depends on ROS-mediated inhibition of PTPase activity in zebrafish. J Hazard Mater. 2021; 412: 125198.
25. Su Q, Su C, Zhang Y, Guo Y, Liu Y, Liu Y, et al. Adjudin protects blood-brain barrier integrity and attenuates

neuroinflammation following intracerebral hemorrhage in mice. Int Immunopharmacol. 2024; 132: 111962.
26. Chen X, Cubillos-Ruiz JR. Endoplasmic reticulum stress signals in the tumour and its microenvironment. Nat Rev Cancer. 2021; 21: 71-88.
27. Lee KW, Hong HR, Lim JS, Ko KP, Lee MG, Chi SG. XAF1 drives apoptotic switch of endoplasmic reticulum stress response through destabilization of GRP78 and CHIP. Cell Death Dis. 2022; 13: 655.
28. Acosta-Alvear D, Harnoss JM, Walter P, Ashkenazi A. Homeostasis control in health and disease by the unfolded protein response. Nat Rev Mol Cell Biol. 2025; 26: 193-212.
29. Yu JE, Yeo IJ, Yoo SS, Kim SH, Son DJ, Yun J, et al. Induction of ER stress-mediated apoptosis through SOD1 upregulation by deficiency of CHI3L1 inhibits lung metastasis. Theranostics. 2023; 13: 2693-709.
30. Congur I, Mingrone G, Guan K. Targeting endoplasmic reticulum stress as a potential therapeutic strategy for diabetic cardiomyopathy. Metabolism. 2025; 162: 156062.
31. Zhang W, Shi Y, Oyang L, Cui S, Li S, Li J, et al. Endoplasmic reticulum stress-a key guardian in cancer. Cell Death Discov. 2024; 10: 343.
32. Marciniak SJ, Chambers JE, Ron D. Pharmacological targeting of endoplasmic reticulum stress in disease. Nat Rev Drug Discov. 2022; 21: 115-40.
33. Choy KW, Murugan D, Mustafa MR. Natural products targeting ER stress pathway for the treatment of cardiovascular diseases. Pharmacol Res. 2018; 132: 119-29.
34. Dan W, Fan Y, Wang Y, Hou T, Wei Y, Liu B, et al. The tumor suppressor TPD52-governed endoplasmic reticulum stress is modulated by APC^{Cdc20}. Adv Sci (Weinh). 2024; 11: e2405441.
35. Fu B, Liu W, Zhu C, Li P, Wang L, Pan L, et al. Circular RNA circBCBM1 promotes breast cancer brain metastasis by modulating miR-125a/BRD4 axis. Int J Biol Sci. 2021; 17: 3104-17.
36. An M, Zang X, Wang J, Kang J, Tan X, Fu B. Comprehensive analysis of differentially expressed long noncoding RNAs, miRNAs and mRNAs in breast cancer brain metastasis. Epigenomics. 2021; 13: 1113-28.
37. Fu B, Zhang A, Li M, Pan L, Tang W, An M, et al. Circular RNA profile of breast cancer brain metastasis: identification of potential biomarkers and therapeutic targets. Epigenomics. 2018; 10: 1619-30.
38. Zhao X, Lei Y, Zheng J, Peng J, Li Y, Yu L, et al. Identification of markers for migrasome detection. Cell Discov. 2019; 5: 27.
39. Chen L, Ma L, Yu L. WGA is a probe for migrasomes. Cell Discov. 2019; 5: 13.
40. Hua J, Chu M, Wang C, Zhang H, Luan J, Zhang Y, et al. Digital PCR-based *GRHL2* methylation testing in acute myeloid leukemia: diagnosis, prognosis and monitoring. Epigenomics. 2024; 16: 233-47.
41. Han B, Zhang H, Tian R, Liu H, Wang Z, Wang Z, et al. Exosomal EPHA2 derived from highly metastatic breast cancer cells promotes angiogenesis by activating the AMPK signaling pathway through Ephrin A1-EPHA2 forward signaling. Theranostics. 2022; 12: 4127-46.
42. Dun MD, Chalkley RJ, Faulkner S, Keene S, Avery-Kiejda KA, Scott RJ, et al. Proteotranscriptomic profiling of 231-BR breast cancer cells: identification of potential biomarkers and therapeutic targets for brain metastasis. Mol Cell Proteomics. 2015; 14: 2316-30.
43. Yang R, Zhang H, Chen S, Lou K, Zhou M, Zhang M, et al. Quantification of urinary podocyte-derived migrasomes for the diagnosis of kidney disease. J Extracell Vesicles. 2024; 13: e12460.
44. Jiang D, Jiang Z, Lu D, Wang X, Liang H, Zhang J, et al. Migrasomes provide regional cues for organ morphogenesis during zebrafish gastrulation. Nat Cell Biol. 2019; 21: 966-77.
45. Yang Y, Lu D, Wang M, Liu G, Feng Y, Ren Y, et al. Endoplasmic reticulum stress and the unfolded protein response: emerging regulators in progression of traumatic brain injury. Cell Death Dis. 2024; 15: 156.
46. da Rocha-Azevedo B, Schmid SL. Migrasomes: a new organelle of migrating cells. Cell Res. 2015; 25: 1-2.
47. Zhao Y, O'Keefe CM, Hsieh K, Cope L, Joyce SC, Pisanic TR, et al. Multiplex digital methylation-specific PCR for noninvasive screening of lung cancer. Adv Sci (Weinh). 2023; 10: e2206518.
48. Jiao H, Jiang D, Hu X, Du W, Ji L, Yang Y, et al. Mitocytosis, a migrasome-mediated mitochondrial quality-control process. Cell. 2021; 184: 2896-910.e13.
49. Shi W, Chen Z, Li L, Liu H, Zhang R, Cheng Q, et al. Unravel the molecular mechanism of XBP1 in regulating the biology of cancer cells. J Cancer. 2019; 10: 2035-46.
50. Ren J, Bi Y, Sowers JR, Hetz C, Zhang Y. Endoplasmic reticulum stress and unfolded protein response in cardiovascular diseases. Nat Rev Cardiol. 2021; 18: 499-521.
51. Krysko DV, Garg AD, Kaczmarek A, Krysko O, Agostinis P, Vandenabeele P. Immunogenic cell death and DAMPs in cancer therapy. Nat Rev Cancer. 2012; 12: 860-75.
52. Banks WA, Hansen KM, Erickson MA, Crews FT. High-mobility group box 1 (HMGB1) crosses the BBB bidirectionally. Brain Behav Immun. 2023; 111: 386-94.
53. Jiao D, Zhang J, Chen P, Guo X, Qiao J, Zhu J, et al. HN1L promotes migration and invasion of breast cancer by up-regulating the expression of HMGB1. J Cell Mol Med. 2021; 25: 397-410.
54. Okura GC, Bharadwaj AG, Waisman DM. Recent advances in molecular and cellular functions of S100A10. Biomolecules. 2023; 13: 1450.
55. Li J, Zhou C, Gao X, Tan T, Zhang M, Li Y, et al. S100A10 promotes cancer metastasis via recruitment of MDSCs within the lungs. Oncoimmunology. 2024; 13: 2381803.
56. Wang X, Huang H, Sze KM, Wang J, Tian L, Lu J, et al. S100A10 promotes HCC development and progression via transfer in extracellular vesicles and regulating their protein cargos. Gut. 2023; 72: 1370-84.
57. Sweeney MD, Kisler K, Montagne A, Toga AW, Zlokovic BV. The role of brain vasculature in neurodegenerative disorders. Nat Neurosci. 2018; 21: 1318-31.

58. Chow BW, Gu C. The molecular constituents of the blood-brain barrier. Trends Neurosci. 2015; 38: 598-608.
59. Li H, Deng Y, Tan M, Feng G, Kuang Y, Li J, et al. Low-intensity pulsed ultrasound upregulates osteogenesis under inflammatory conditions in periodontal ligament stem cells through unfolded protein response. Stem Cell Res Ther. 2020; 11: 215.
60. Zhang B, Cao JT, Wu YB, Gao KX, Xie M, Zhou ZK, et al. Riboflavin (Vitamin B2) deficiency induces apoptosis mediated by endoplasmic reticulum stress and the CHOP pathway in HepG2 cells. Nutrients. 2022; 14: 3356.
61. Luo T, Chen B, Wang X. 4-PBA prevents pressure overload-induced myocardial hypertrophy and interstitial fibrosis by attenuating endoplasmic reticulum stress. Chem Biol Interact. 2015; 242: 99-106.
62. Luo T, Kim JK, Chen B, Abdel-Latif A, Kitakaze M, Yan L. Attenuation of ER stress prevents post-infarction-induced cardiac rupture and remodeling by modulating both cardiac apoptosis and fibrosis. Chem Biol Interact. 2015; 225: 90-8.
63. van Niel G, Carter DRF, Clayton A, Lambert DW, Raposo G, Vader P. Challenges and directions in studying cell-cell communication by extracellular vesicles. Nat Rev Mol Cell Biol. 2022; 23: 369-82.
64. Marar C, Starich B, Wirtz D. Extracellular vesicles in immunomodulation and tumor progression. Nat Immunol. 2021; 22: 560-70.
65. Wen N, Peng D, Xiong X, Liu G, Nie G, Wang Y, et al. Cholangiocarcinoma combined with biliary obstruction: an exosomal circRNA signature for diagnosis and early recurrence monitoring. Signal Transduct Target Ther. 2024; 9: 107.
66. Zhang L, Parvin R, Fan Q, Ye F. Emerging digital PCR technology in precision medicine. Biosens Bioelectron. 2022; 211: 114344.
67. Sirenko M, Bernard E, Creignou M, Domenico D, Farina A, Arango Ossa JE, et al. Molecular and clinical presentation of UBA1-mutated myelodysplastic syndromes. Blood. 2024; 144: 1221-9.
68. Merino I, de la Fuente A, Domínguez-Gil M, Eiros JM, Tedim AP, Bermejo-Martín JF. Digital PCR applications for the diagnosis and management of infection in critical care medicine. Crit Care. 2022; 26: 63.

Cite this article as: Wang S, Gu G, Xian X, Li J, Zhang D, Guo J, et al. Cancer cell-derived migrasomes harboring ATF6 promote breast cancer brain metastasis *via* endoplasmic reticulum stress-mediated disruption of the blood-brain barrier. Cancer Biol Med. 2025; 22: 690-713. doi: 10.20892/j.issn.2095-3941.2025.0014